

Mechanical Design and Control of Flexible-Legged Jumping Robots

A Thesis

Presented to the

Graduate Faculty of the

University of Louisiana at Lafayette

In Partial Fulfillment of the

Requirements for the Degree

Masters of Science

Andrew Albright

Spring 2022

© Andrew Albright

2022

All Rights Reserved

Mechanical Design and Control of Flexible-Legged Jumping Robots

Andrew Albright

APPROVED:

---

Joshua E. Vaughan, Chair  
Assistant Professor of Mechanical  
Engineering

---

Anthony S. Maida  
Associate Professor of Computer  
Science

---

Alan A. Barhorst  
Department Head of Mechanical  
Engineering

---

Mary Farmer-Kaiser  
Dean of the Graduate School

*To all the poor souls using Word, one day you will see the light that is L<sup>A</sup>T<sub>E</sub>X.*

*“Before we work on artificial intelligence why don’t we do something about natural  
stupidity?”*

— Steve Polyak

## Acknowledgments

I would like to firstly thank my advisor Dr. Joshua Vaughan for his leadership, both academic and personal, during my time here at the university. His support has been invaluable in helping me to understand the underlying ideas behind this material. Additionally, his constant drive to produce high quality material has kept me motivated in my attempts to do the same. I would not be here without him.

Additionally, I would like to thank my committee members, Dr. Alan Barhorst, Dr. Anthony Maida and Dr. Brian Post for their input in regards to this work. Along with my lab members during my time in the C.R.A.W.L.A.B., Gerald Eaglin, Adam Smith, Y (Eve) Dang, Brennan Moeller and Darcy LaFont. Their conversations and advice have greatly assisted me in my efforts to complete this work.

Lastly, I would like to thank the Louisiana Crawfish Board for their financial support in the form of a grant from the University of Louisiana at Lafayette. This grant has allowed me to work knowing my fiscal security was in tact.

## Table of Contents

Dedication . . . . .	iv
Epigraph . . . . .	v
Acknowledgments . . . . .	vi
List of Tables . . . . .	ix
List of Figures . . . . .	x
<b>I Introduction and System Description . . . . .</b>	<b>1</b>
1.1 Improving Performance with Flexible Components . . . . .	2
1.2 Controlling Flexible Systems . . . . .	3
1.3 Concurrent Design . . . . .	3
1.4 Reinforcement Learning . . . . .	4
1.5 Twin Delayed Deep Deterministic Policy Gradient . . . . .	5
1.6 Contributions . . . . .	9
<b>II Learning Efficient Jumping Strategies for the Monopode System . . . . .</b>	<b>11</b>
2.1 Monopode Jumping System . . . . .	11
2.2 Training Environment . . . . .	13
2.3 Efficient Control Strategies . . . . .	15
2.4 Deploying TD3 . . . . .	16
2.5 Average Performance of Network Controller . . . . .	17
2.5.1 Input Commands . . . . .	17
2.5.2 Jumping Height Performance . . . . .	19
2.5.3 Height Reached vs. Power Used . . . . .	20
2.6 Optimal Performance of Network Controller . . . . .	21
2.6.1 Input Commands . . . . .	21
2.6.2 Jumping Height Performance . . . . .	22
2.7 Conclusion . . . . .	23
<b>III Using Input Shaping to Validate RL Controller . . . . .</b>	<b>25</b>
3.1 Input Shaping Controller Input . . . . .	26
3.2 RL Controller Input . . . . .	27
3.3 Conclusion . . . . .	27
<b>IV Mechanical Design of a the Monopode Jumping System . . . . .</b>	<b>28</b>
4.1 Learning a Mechanical Design . . . . .	28
4.2 Environment Definition . . . . .	29
4.3 Rewards for Learning Designs . . . . .	30
4.4 Design Space Variations . . . . .	30
4.5 Deploying TD3 . . . . .	32

<b>4.6</b>	<b>Jumping Performance . . . . .</b>	<b>33</b>
4.6.1	Narrow Design Space . . . . .	33
4.6.2	Wide Design Space . . . . .	35
4.6.3	Average Design Performance . . . . .	37
<b>4.7</b>	<b>Conclusion . . . . .</b>	<b>38</b>
<b>V</b>	<b>Concurrent Design of the Monopode System . . . . .</b>	<b>39</b>
5.1	Concurrent Design Architecture . . . . .	39
5.2	Mechanical Design Update . . . . .	40
5.2.1	Discrete vs. Continuous . . . . .	40
5.2.2	Averaging $n$ Design Policies . . . . .	40
5.2.3	Differing Reward Types . . . . .	40
5.2.4	Design Update Rate . . . . .	41
5.3	Environment Definition . . . . .	41
5.3.1	Learning the Controller . . . . .	41
5.3.2	Learning the Design . . . . .	42
5.4	Deploying the Algorithm . . . . .	43
5.5	Mechanical Designs . . . . .	44
5.6	Controller Performance . . . . .	45
5.7	Conclusion . . . . .	47
<b>VI</b>	<b>Appendix: Concurrent Design Algorithm . . . . .</b>	<b>48</b>
6.0.1	Additional Hyperparameters . . . . .	48
6.0.2	Discrete vs. Continuous . . . . .	48
<b>Bibliography</b>	. . . . .	<b>53</b>
<b>Abstract</b>	. . . . .	<b>57</b>
<b>Biographical Sketch</b>	. . . . .	<b>58</b>

## List of Tables

<b>Table 1.</b>	Monopode Model Parameters . . . . .	12
<b>Table 2.</b>	TD3 Training Hyperparameters . . . . .	17
<b>Table 3.</b>	TD3 Training Hyperparameters . . . . .	32
<b>Table 4.</b>	Learned Design Parameters . . . . .	37
<b>Table 5.</b>	Outer Loop TD3 Training Hyperparameters . . . . .	43
<b>Table 6.</b>	TD3 Training Hyperparameters . . . . .	44

## List of Figures

<b>Figure 1.</b> Flexible Robotics System . . . . .	1
<b>Figure 2.</b> Rotary Style Series Elastic Actuator . . . . .	2
<b>Figure 3.</b> Tendon Like Flexibility from [1] . . . . .	2
<b>Figure 4.</b> Reinforcement Learning Process . . . . .	5
<b>Figure 5.</b> Twin Delayed Deep Deterministic Policy Gradient Block Diagram with Monopode as Environment . . . . .	6
<b>Figure 6.</b> Monopode Jumping System . . . . .	12
<b>Figure 7.</b> Jumping Types for the Monopode Jumping System . . . . .	14
<b>Figure 8.</b> Reward vs Time Step During Training . . . . .	17
<b>Figure 9.</b> Average and Standard Deviation Inputs to monopode . . . . .	18
<b>Figure 10.</b> Average and Standard Deviation Heights of monopode . . . . .	19
<b>Figure 11.</b> Height Reached vs Power Consumed of monopode . . . . .	20
<b>Figure 12.</b> Optimal Inputs to monopode . . . . .	21
<b>Figure 13.</b> Optimal Heights of monopode . . . . .	23
<b>Figure 14.</b> Jumping Command . . . . .	25
<b>Figure 15.</b> Resulting Actuator Motion . . . . .	26
<b>Figure 16.</b> Decomposition of the Jump Command into a Step Convolved with an Impulse Sequence . . . . .	26
<b>Figure 17.</b> Jumping Performance of Narrow Design Space . . . . .	31
<b>Figure 18.</b> Jumping Performance of Broad Design Space . . . . .	31
<b>Figure 19.</b> Reward vs. Episode for Learning Mechanical Design . . . . .	32
<b>Figure 20.</b> Height Reached During Training . . . . .	33
<b>Figure 21.</b> Spring Constant Selected During Training . . . . .	34

<b>Figure 22.</b> Damping Ratio Selected During Training . . . . .	34
<b>Figure 23.</b> Height Reached During Training . . . . .	35
<b>Figure 24.</b> Spring Constant Selected During Training . . . . .	36
<b>Figure 25.</b> Damping Ratio Selected During Training . . . . .	36
<b>Figure 26.</b> Height vs Time of Average Optimal Designs . . . . .	37
<b>Figure 27.</b> Designs Learned Using Update Rate = 1:500 Control Policy Updates	45
<b>Figure 28.</b> Average Input Performance . . . . .	46
<b>Figure 29.</b> Average Jumping Performance . . . . .	46

## I Introduction and System Description

A legged locomotive robot can have many advantages over a wheeled or tracked one, particularly in regards to their ability to navigate uneven and unpredictable terrain [2, 3]. They can achieve this advantage because of the numerous movement types they can deploy. Abilities such as independently placing their feet within highly rigid terrain and jumping or bounding over obstacles have been shown to be effective ways of locomoting [4]. These advantages do not come at no cost, however. Legged systems are traditionally power inefficient compared to wheeled vehicles making them a less attractive option for applications where power conservation is required. Research has been conducted showing the usefulness of adding flexible components, like the legs seen on the robot in Figure 1, for combating efficiency and other issues [3, 5, 6]. The addition of these components in legged robots has been shown to increase system performance measures such as running speed, jumping capability and power efficiency [7]. However, the addition of flexible components creates a system that is highly nonlinear, and thus requires a more complex control system.



**Figure 1.** Flexible Robotics System

## 1.1 Improving Performance with Flexible Components

The use of flexible components within robotic systems has been shown to be an effective way of improving performance metrics such as movement velocity and power efficiency [3, 7]. Of the different techniques that have been deployed, the use of series elastic actuators (SEAs) has been shown to be an effective for increasing energy efficiency [8, 9]. Storing energy in the non-rigid parts of motor joints, such as the spring seen in Figure 2, have proven to be an effective way in increasing efficiency. The addition of flexible joints is not the only technique that has been used to improve performance, however; utilizing tendon like elastic members to connect actuators to links has also been shown to be an effective way of improving efficiency [1]. The use of tendons, being an example of replicating what is found in nature, is a common method

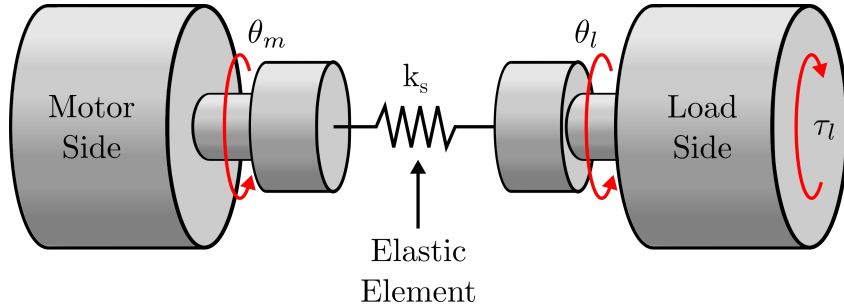


**Figure 2.** Rotary Style Series Elastic Actuator

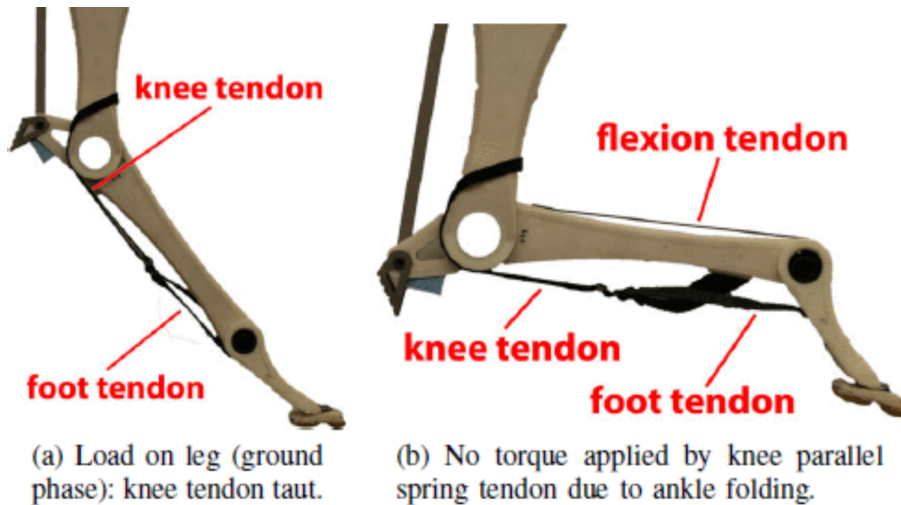


**Figure 3.** Tendon Like Flexibility from [1]

of finding unique mechanical designs that perform well in the real world. An example of this type of design can be seen in Figure 3. Following a similar idea, research has also been conducted finding the usefulness of including flexibility in the spine of 2D running robots where the velocity of the robot was drastically increased [10]. Research studying the effects of flexible links, like the ones shown in Figure 1 is limited though, particularly in the realm of legged-robots. Still, it has been shown as a viable method of increasing performance in these types of robots [11].

## 1.2 Controlling Flexible Systems

Control methods developed for flexible systems have been shown to be effective for position control and vibration reduction [9, 12]. Because of the challenges seen in scaling the controllers, methods utilizing reinforcement learning are of interest. This method has been used in simple planar cases, where it was compared to a PD control strategy for vibration suppression and proved to be a higher performing method [13]. Additionally, it has also been shown to be effective at defining control strategies for flexible-legged locomotion. The use of actor-critic algorithms such as Deep Deterministic Policy Gradient [14] have been used to train running strategies for a flexible legged quadruped [15]. Much of the research is based in simulation, however, and often the controllers are not deployed on physical systems, which leads to the question of whether or not these are useful techniques in practice.

## 1.3 Concurrent Design

Defining an optimal controller for a system can be difficult due to challenges such as mechanical and electrical design limits. This is especially true when the system is flexible and the model is nonlinear. A solution to this challenge is to concurrently design a system with the controllers so that the two are jointly optimized. Defining the design process such that the robot's design results in a simple dynamic model has been shown to improve the performance of mechatronics systems [16]. Additionally, in more

recent work, the utilization of more complex deep learning methods have shown to be an effective strategy for finding optimal concurrent designs [17]. Deep learning has been used to find a concurrent designs for simulated legged robotic systems leading to improved performance in regards to movement velocity [18]. Some research has even been completed where the designs were deployed on physical hardware, validating that this area of research is an effective one for learning how best to define system/controller architectures [19]. Little research exists however, utilizing these techniques on legged-robotic systems, particularly ones that are flexible in nature.

## 1.4 Reinforcement Learning

With the recent successes seen in utilizing reinforcement learning (RL) to define control strategies, design parameters and concurrent designs for robot systems, it is of interest to apply this technique in a unique way to flexible-legged jumping systems. Firstly, it is important to understand the generalities regarding a reinforcement learning problem.

Reinforcement Learning is the process of training a policy to define a series of commands using an environment where those commands can be applied. A policy, often referred to as an agent, from a controls theory perspective, is synonymous with a controller. The environment the controller is deployed in, again from a controls theory perspective, is synonymous with a robotic system. Training the controller requires iteratively deploying the controller's commands, or actions, to the the environment and observing the results. The results are often in the form of the state of the environment and a reward resulting from the action that was applied. The reward is defined by the designer so that the controller is trained to accomplish a desired task. Other than the reward, the controller has no way to decern what commands are good when the environment is in some state. The iterative learning process is often described using the block diagram shown in Figure 4.

Learning an optimal control strategy to accomplish a task is completed by deploying a gradient decent based learning algorithm utilizing information such as the state of the environment and the reward. For general robotics applications, at each discrete time step  $t$ , the environment will be in a state  $s \in \mathcal{S}$ , the controller will select an action  $a \in \mathcal{A}$  according to the current policy  $\pi : \mathcal{S} \rightarrow \mathcal{A}$ , and apply said action within the environment. The environment will transition to a new state  $s'$  and will generate a reward  $r$  based on the users definition. The return, being the value the algorithm is trying top optimize, is defined as a discounted sum of rewards,  $R_t = \sum_{i=t}^T \gamma^{i-t} r(s_i, a_i)$ , where  $\gamma$  is a discount factor for discerning between giving importance to near-term or long-term rewards.

The challenge of an RL algorithm is to optimize a policy,  $\pi_\phi$ , with parameters,  $\phi$ , such that actions generated at each time step will maximize the return. Ultimately, an optimized policy will maximize the expected return,  $J(\phi) = \mathbb{E}_{s_i \sim p_\pi, a_i \sim \pi}[R_0]$ .

## 1.5 Twin Delayed Deep Deterministic Policy Gradient

There are many algorithms used to train a network based controller in an RL application, some of which have shown their ability to learn high performing control strategies for robotics systems [20–22]. Of the different algorithms used in research today, the one selected and tested in this work is Twin Delayed Deep Deterministic Policy Gradient (TD3) [23]. This is an actor-critic type learning algorithm which is

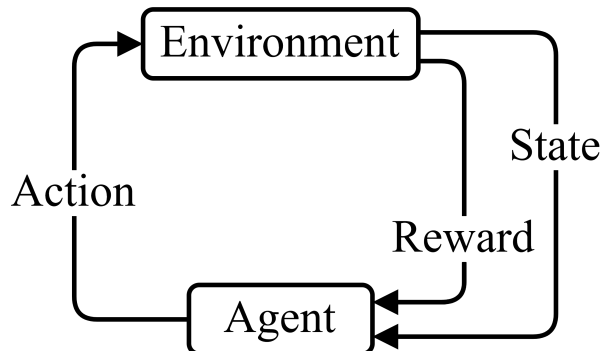


**Figure 4.** Reinforcement Learning Process

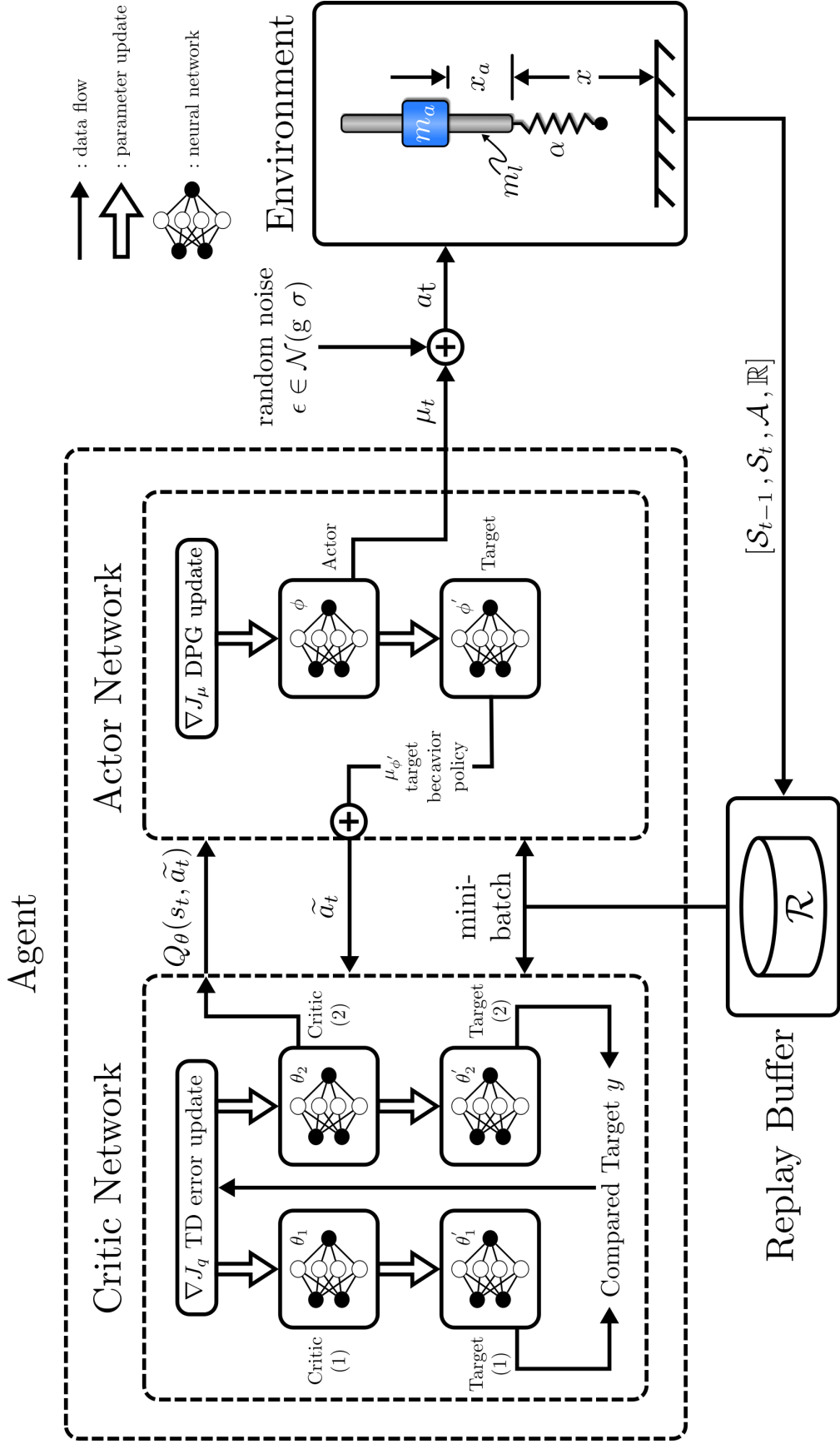


Figure 5. Twin Delayed Deep Deterministic Policy Gradient Block Diagram with Monopode as Environment

widely considered the predecessor to the popular and proven Deep Deterministic Policy Gradient (DDPG) algorithm [14].

Figure 5 displays the flow in information for this algorithm. In general, this algorithm learns both a Q-function and a policy, being the *critic* and the *actor*. The Q-function is updated in an off-policy fashion using data stored in a replay buffer. A technique finding the temporal difference error between the target Q-function and the main Q-function is used to minimize a loss function. For algorithms such as TD3, the ultimate goal is to find a policy,  $\pi_\theta$ , which maximizes the expected return:

$$\nabla_\phi J(\phi) = \mathbb{E}_{s \sim p_\pi} [\nabla_a Q^\pi(s, a)|_{a=\pi(s)} \nabla_\phi \pi_\phi(s)] \quad (1)$$

where  $Q^\pi(s, a) = \mathbb{E}_{s_i \sim p_\pi, a_i \sim \pi}[R_t | s, a]$  is the value function and the critic in the case of the TD3 architecture. Updating the Q-function, again, is accomplished using temporal difference between the Q-function and a target Q-function [24, 25], both which are based on the Bellman Equation:

$$Q^\pi(s, a) = \mathbb{E}_{s' \sim P} \left[ r(s, a) + \gamma \max_{a'} Q^\pi(s', a') \right] \quad (2)$$

Using a differentiable function approximator,  $Q^\pi(s, a)$  can be represented and estimated using by  $Q_\phi(s, a)$ , with parameters  $\phi$  [26]. To maintain a fixed objective over multiple policy updates, the target Q-function approximator is instantiated separately as  $Q_{\phi_{targ}}(s, a)$ . The target does depend on the same parameters that are being trained,  $\phi$ , where there exists an issue when trying to use it as a target. To solve this issue the target network is updated at a delayed pace following the main Q-function approximator by either matching the parameters or by polyak averaging,  $\phi_{targ} \leftarrow \tau\phi + (1 - \tau)\phi_{targ}$ , where  $\tau$  is a tunable hyperparameter.

Summing it up then, the critic side of the TD3 algorithm is responsible for minimizing the difference between the value of the current state/action pair using the main Q-function, and the reward of the current state/action pair plus the discounted value of the next state/action pair using the target Q-function. The loss function takes

the form:

$$L(\phi, \mathcal{D}) = \underset{(s,a,r,s',d) \sim D}{E} \left[ (Q_\phi(s, a) - (r(s, a) + \gamma(1-d) Q_{\phi_{targ}}(s', \pi_{\theta_{targ}}(s'))))^2 \right] \quad (3)$$

where  $\pi_{\theta_{targ}}(s')$  is a target policy that, in a similar manner to the target Q-function, follows the main policy,  $\pi_\theta$ , at a delayed pace either by directly copying the values or by polyak averaging. Additionally,  $d$  represents a boolean value which depends on the terminal status of the next state,  $s'$ .

As for updating the policy for the actor critic-type algorithm, this aspect is rather simple. Because DDPG, and therefore TD3, are built to accommodate only continuous action spaces, the Q-function is assumed to be differentiable with respect to action. Therefore to find optimal policy parameters,  $\theta$ , for the policy,  $\pi_\theta$ , the solution of the following equation must be found:

$$\max_{\theta} \underset{s \sim D}{E} [Q_\phi(s, \pi_\theta(s))] \quad (4)$$

The reason that TD3 is considered the predecessor to DDPG, is that there are some additional tricks deployed in addition to the description thus far. The first being the addition noise to the target policy. It can be seen in Equation 3 that the target policy,  $\pi_{\theta_{targ}}$ , is required to generate an action to evaluate the target Q-function. Noise is added to the policy taking the form:

$$a'(s') = \text{clip} (\pi_{\theta_{targ}}(s') + \text{clip}(\epsilon, -c, c), a_{low}, a_{high}), \quad \epsilon \sim \mathcal{N}(0, \sigma) \quad (5)$$

where  $\epsilon$  represents the noise sampled in some form that the user can specify. This method of adding noise was shown by the authors of the algorithm to reduce a known issue where the Q-function approximator can develop large peaks for certain actions.

The second trick the TD3 algorithm deploys is the addition of a second Q-function approximator and target Q-function approximator. A known potential issue of the Q-function is that it can suffer from overestimation of the value of action/state

pairs. This of course leads to the policy learning actions that the Q-function assumes are better than they actually are. To alleviate this issue, the authors suggest instantiating two Q-functions and two target Q-functions. Calculate the two target Q-functions:

$$y(r, s', d) = r(s, a) + \gamma (1 - d) Q_{\phi_{1,targ}}(s', \pi_{\theta_{targ}}(s')) \quad (6)$$

and take the lower of the two targets to update both the main Q-functions:

$$L(\phi_1, \mathcal{D}) = \underset{(s,a,r,s',d) \sim D}{E} \left[ (Q_{\phi_1}(s, a) - y(r, s', d))^2 \right] \quad (7)$$

$$L(\phi_2, \mathcal{D}) = \underset{(s,a,r,s',d) \sim D}{E} \left[ (Q_{\phi_2}(s, a) - y(r, s', d))^2 \right] \quad (8)$$

.  
The last trick that the TD3 algorithm deploys is the addition of a delay between the update of the Q-functions and the policy. They found that in doing this, the Q-function was able to converge to a better solution before updating the policy. Ultimately, the addition of a policy update delay was done to reduce coupling between the Q-function and the policy. The recommended delay the authors suggest is updating the policy every two Q-function updates.

There are many implementations of the TD3 algorithm that are available, however the StableBaselines3 implementation is used to complete the work in this thesis [27]. StableBaselines3 is a widely popular library of RL algorithm implementations, and is composed of well written and understandable documentation for the supported implementations. The differentiable function approximators used to estimate the policies and Q-functions are built within StableBaselines3 using PyTorch [28], which is also a widely popular framework for machine learning and more specifically reinforcement learning.

## 1.6 Contributions

The purpose of the work presented in the remainder of the document is to evaluate and present the performance of a concurrent design architecture that utilizes

RL techniques, for flexible jumping systems. In doing this, the method will be divided into multiple sections wherein additional findings will be presented.

In the next Chapter, a RL based controller will be trained on a flexible jumping system to evaluate the effectiveness of training for efficient control. Power use is often considered when designing RL controllers for rigid systems, typically taking the form of a weighted negative reward when deploying an RL algorithm. It is of interest to evaluate if defining strategies, with efficiency being the primary objective, for flexible systems, if the resulting control strategy takes advantage of system flexibility. In Chapter 3, more traditional methods are used to evaluate the changes in control strategies when training a controller to consider efficiency.

In Chapter 4, a RL problem is defined in a unique way such that the environment the policy is deployed in is a simulation of an environment where the actions sent by the policy are mechanical design updates. It is of interest to evaluate if an RL based approach can be taken to learn mechanical design parameters of a flexible jumping system, such as flexibility. Furthermore, using a single fixed control input, it is of interest to determine if this technique can be used to define designs to accomplish multiple tasks. Finally, in Chapter 5, the methods of learning a control strategy and learning a design will be combined to create a concurrent design technique. The resulting designs and controller performance will be presented and the method will be evaluated.

## II Learning Efficient Jumping Strategies for the Monopode System

Utilizing reinforcement learning to train a neural network based controller has been shown to be useful for controlling many robotic systems [21, 22]. It has been used to successfully control rigid-legged robots both in simulation and on physical hardware [20, 29]. Reinforcement learning has been shown to be capable of defining more effective and efficient jumping techniques for a single-legged robot with SEAs [30]. It has also been shown to be an effective method for controlling multi-legged robots both in simulation and on physical hardware [31–33]. Furthermore, it has been shown to be useful for defining energy efficient strategies for multi-legged robots that have been deployed on physical hardware [34]. However, the body of work demonstrating the use of RL to train controllers for flexible systems is limited, particularly in regards to legged locomotive systems. In this Chapter, RL is deployed to define an energy efficient jumping strategy for a monopode jumping. The purpose of this work is to validate the use of RL for defining the control aspect of a concurrent design architecture for flexible jumping systems.

### 2.1 Monopode Jumping System

To evaluate the methods discussed in this Chapter, a monopode system like the one shown in Figure 6 was used to represent a flexible jumping system. This system has been studied and has been proven to be an effective base for modeling the jumping gaits for many different animals [35].

The monopode is controlled by accelerating the actuator mass,  $m_a$ , along the rod mass,  $m_l$ , causing a hopping like motion. The system contacts the ground through a nonlinear spring, represented by the variable  $\alpha$  in the figure. Also included in the model is a damper parallel with the spring, having a damping coefficient of  $c$ , though it is not shown in the figure. Variables  $x$  and  $x_a$  represent the rod's global position and the actuator's local position with respect to the rod, respectively. The equation of

motion for the system is:

$$\ddot{x} = \frac{\gamma}{m_t} (\alpha x + \beta x^3 + c \dot{x}) - \frac{m_a}{m_t} \ddot{x}_a - g \quad (9)$$

where  $x$  and  $\dot{x}$  are position and velocity of the rod, respectively, the acceleration of the actuator,  $\ddot{x}_a$ , is the control input, and  $m_t$  is the mass of the complete system.

Constants  $\alpha$  and  $c$  represent the linear spring and damping coefficient, respectively, and constant  $\beta$  is set to  $1e8$ . Ground contact determines the value of  $\gamma$ , so that the spring

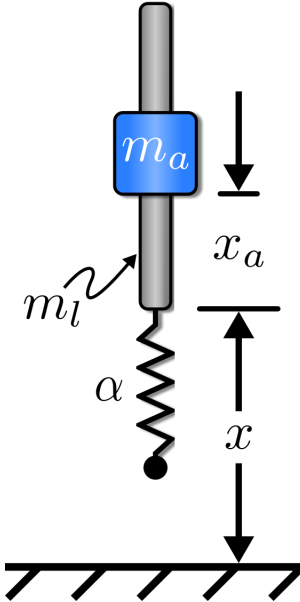


**Figure 6.** Monopode Jumping System

**Table 1.** Monopode Model Parameters

Model Parameter	Value
Mass of Leg, $m_l$	0.175 kg
Mass of Actuator, $m_a$	1.003 kg
Spring Constant, $\alpha_{nominal}$	5760 N/m
Natural Frequency, $\omega_n$	$\sqrt{\frac{\alpha}{m_l+m_a}}$
Damping Ratio, $\zeta_{nominal}$	$1e-2 \frac{\text{N}}{\text{m/s}}$
Gravity, $g$	9.81 m/s <sup>2</sup>
Actuator Stroke, $(x_a)_{\max}$	0.008 m
Max. Actuator Velocity, $(\dot{x}_a)_{\max}$	1.0 m/s
Max. Actuator Acceleration, $(\ddot{x}_a)_{\max}$	10.0 m/s <sup>2</sup>

and damper do not supply force while the leg is airborne:

$$\gamma = \begin{cases} -1, & x \leq 0 \\ 0, & \text{otherwise} \end{cases} \quad (10)$$

Additionally, the spring compression limit, or the systems position in the negative  $x$  direction, is limited to 0.008m. Finally, the system is confined to move only vertically in regards to Figure 6 so that controlling ballance is not required.

## 2.2 Training Environment

Using the monopode model, a traditional RL environment aligning with the standards set by OpenAI for a Gym environment was created [36]. The observation and action spaces were defined, respectively, as follows:

$$\mathcal{S} = [x_{at}, \dot{x}_{at}, x_t, \dot{x}_t] \quad (11)$$

$$\mathcal{A} = [\ddot{x}_{at}] \quad (12)$$

where  $x_t$ ,  $\dot{x}_t$  were the monopode's position and velocity at time  $t$ , and  $x_{at}$ ,  $\dot{x}_{at}$  and  $\ddot{x}_{at}$  were the actuator's position, velocity and acceleration, respectively.

Two separate stopping conditions were defined for the environment to evaluate two different jump types and therefore two different input commands. The first was defined as the monopode's position being greater than zero than returning to zero once. The second was defined like the first but with the monopode's position being greater than zero and then less than zero twice.

Two different jumps are create from these stopping conditions. The first was referred to as a single jump command, and the second a stutter jump command. The intent of utilizing two different jumping commands was to determine if a RL algorithm was more or less effective in learning differing strategies depending on the complexity of the desired command.

An example single jump can be seen in Figure 7a. The intended command from the learned controller would be one that would jump the monopode once. This type of

command would ideally compress the spring/damper by accelerating the actuator in the positive direction. This would allow the system to store energy in the spring that could be used to cause the system to jump. The actuator mass should then accelerate downward forcing the spring to decompress. At this point, the system should be accelerating upwards and the actuator downwards such that the monopode leaves the

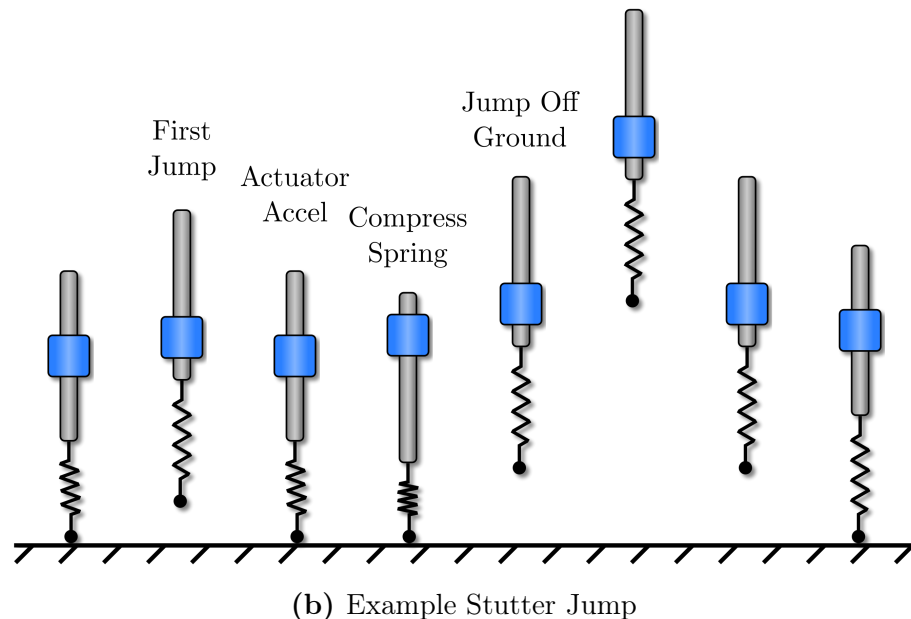
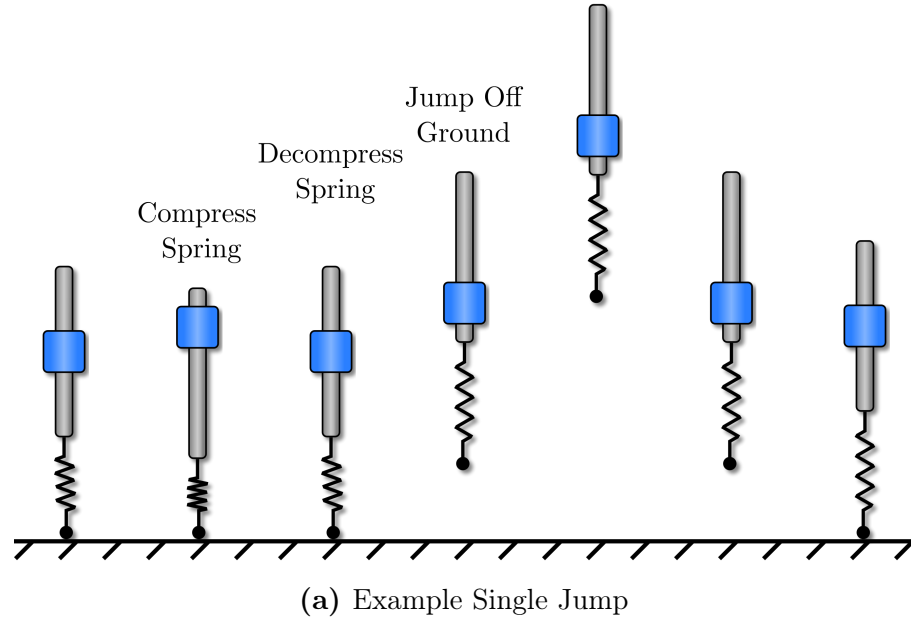


**Figure 7.** Jumping Types for the Monopode Jumping System

ground completing a single jump.

An example stutter jump can be seen in Figure 7b. The intended command from the learned controller would be one that would jump the monopode twice. This type of command would firstly complete an optimal single jump. Following that motion, the actuator should assume an acceleration direction to recompress the spring storing more energy with a farther compression. When the spring is compressed to its maximum value or the system’s total acceleration reaches zero, the actuator mass should accelerate downwards forcing the spring to decompress. At this point, the system should be accelerating upwards and the actuator downwards, similar to the single jump, such that the monopode leaves the ground completing a stutter jump.

### 2.3 Efficient Control Strategies

Efficient control of a robotic system is often one of the most important aspects of a controller’s design. Applications where a robotic system is deployed and relies on a limited power source, such as a mobile walking robot, will often require an efficient control strategy. Modern, traditional methods, such as model predictive control, have been shown to produce energy efficient locomotion strategies for wheeled and legged systems [37, 38]. It is of interest in this work to utilize RL, a modern neural network based control method, to find strategies which are designed with power efficiency as the primary objective.

Two different reward functions were designed to accomplish the task of determining how well RL learns efficient jumping strategies. The purpose of defining two different reward functions was to compare the input commands and resulting jumping shapes of the two controller types to determine if the efficient controller was learning to conserve power.

The first reward function was one that ignored power usage and focused solely

on the height of the jump:

$$R = x_t \quad (13)$$

where  $x_t$  was the height of the monopode system at any given time step. The second reward function was one that was defined to accomplish the same task, but also consider power consumption and was defined as:

$$R = \frac{x_t}{\sum_{t=0}^t P_t} \quad (14)$$

where  $P_t$  was the power consumption of the monopode system at any given time step defined mechanically as the product of the actuator's acceleration, velocity and mass:

$$P_t = m_a \dot{x}_a \ddot{x}_a \quad (15)$$

where  $m_a$  was the mass of the actuator, and  $\dot{x}_a$  and  $\ddot{x}_a$  where the actuators velocity and acceleration, respectively.

## 2.4 Deploying TD3

Because training an RL controller does not guarantee that the controller will learn an optimal strategy without finding local optima, training more than one controller is often practiced to evaluate performance. In this work, fifty different controllers where trained, each with a different random network initialization. Each controller was trained for a total 500k time steps. The remaining hyperparameters set using the TD3 algorithm are defined in Table 2.

The rewards the TD3 algorithm received during training are presented in Figure 8. They represent the controllers being trained to accomplish their respective goals. Looking at Figure 8a, which shows the rewards for learning a single jumping command, it is clear that there are stark differences between the efficient and high jumping reward types. Firstly, the high jumping strategy does converge after 500k steps of training. The reward for the efficient jumping controller, having been defined drastically different than the reward from the high jumping controller, not surprisingly,

looks drastically different than the high jumping reward. The reward for the efficient agent is heavily punished for using power without gaining height, which is a frequent occurrence in the beginning of training. This allows the policy to learn quickly that using less power will result in a higher rewards which is shown in the training reward data. Looking at Figure 8b, it is also apparent that the height controller is converging to a solution. Additionally, the efficient controller can be seen to have learned in the same rapid form as the single jumping command type.

**Table 2.** TD3 Training Hyperparameters

Hyperparameter	Value
Learning Rate, $\alpha$	0.001
Learning Starts	1000 Steps
Batch Size	100 Transitions
Tau, $\tau$	0.005
Gamma, $\gamma$	0.99
Training Frequency	1:Episode
Gradient Steps	$\propto$ Training Frequency
Action Noise, $\epsilon$	None
Policy Delay	1 : 2 Q-Function Updates
Target Policy Noise, $\epsilon$	0.2
Target Policy Clip, $c$	0.5
Seed	50 Random Seeds

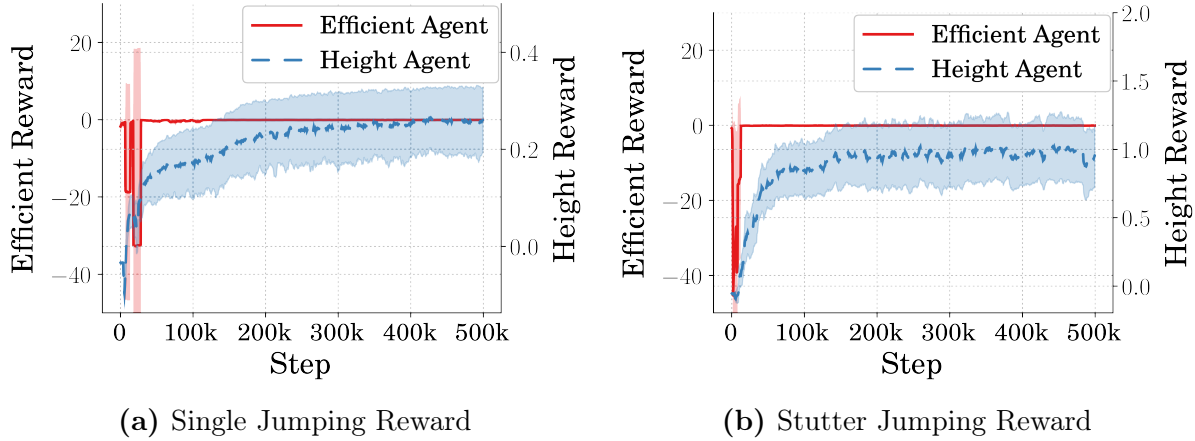


**Figure 8.** Reward vs Time Step During Training

## 2.5 Average Performance of Network Controller

**2.5.1 Input Commands.** Average learned input commands for both the single and stutter jumping cases are shown in Figure 9 to compare controllers that were trained to jump efficiently to those trained to jump high. At first glance, there are obvious differences regarding timing, magnitude and direction. There are also slight differences in variance seen between the two controller types. Starting with Figure 9a, which displays the input commands for the single jumping case, it is most obvious that the direction for the initial acceleration of the actuator mass for the efficient controllers and height controllers differ. In the case where the controller is learning to jump high, an initial acceleration in the negative direction is learned, which contrasts the case where the controller is learning an efficient command. Further, the magnitude of the commands is drastically different which may be an indicator for conserving power. Looking now at Figure 9b, it is immediately apparent that the magnitudes of the commands differ greatly. They are however, more similar in regards to their timings and directions when comparing the stutter jumping command to the single jumping command. In both the single and stutter jumping cases, it can be seen that there is upward acceleration command towards the end of the jump, which again might be an indicator of a more efficient jumping strategy. Furthermore, it can be observed that the

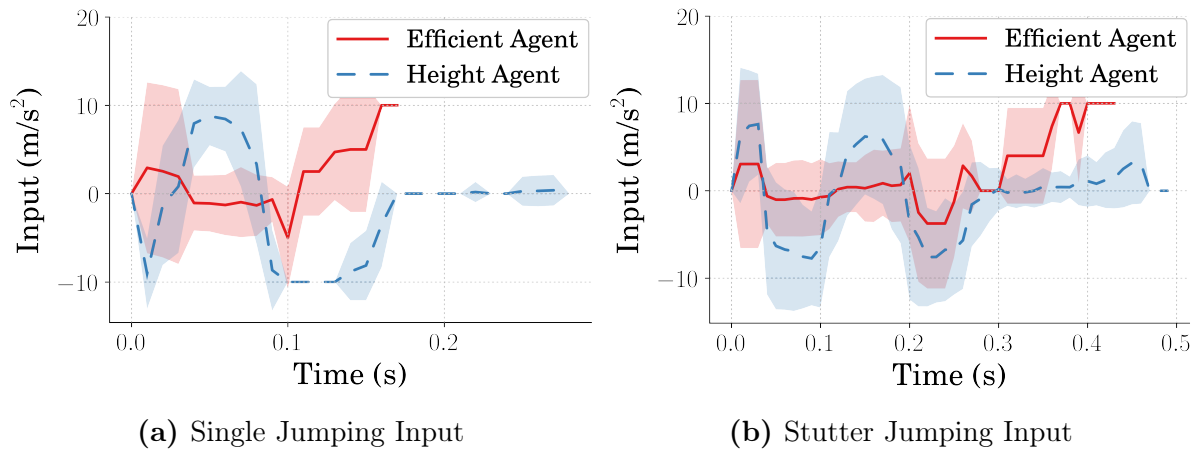


**Figure 9.** Average and Standard Deviation Inputs to monopode

single jumping case, there exists more variance across different instances of the trained efficient controllers in comparison to the height controllers. This does not seem to be the case for the stutter jumping command type, though both cases do seem to generate controllers with high variance inputs across instances.

**2.5.2 Jumping Height Performance.** Average jumping performance resulting from the learned single and stutter jumping commands is displayed in Figure 10. In both the single and stutter jumping cases, there are differences seen in jumping ability when comparing the efficient and height controller types. At first glance it is apparent that when increasing the complexity of the command from a single jump to a stutter jump, the efficient controllers are better able to replicate the performance of the height controllers.

Starting with Figure 10a, it is most apparent that the height controllers learned a command input that was outperformed the efficient controllers in terms of jump height. The resulting motion from the input discussed in the previous section can also be seen in that the efficient controller learned to simply compress the spring, then jump the monopode. The height controllers, in contrast, disregarding power consumption, learned to decompress the spring from its nominal position, keeping it below the point

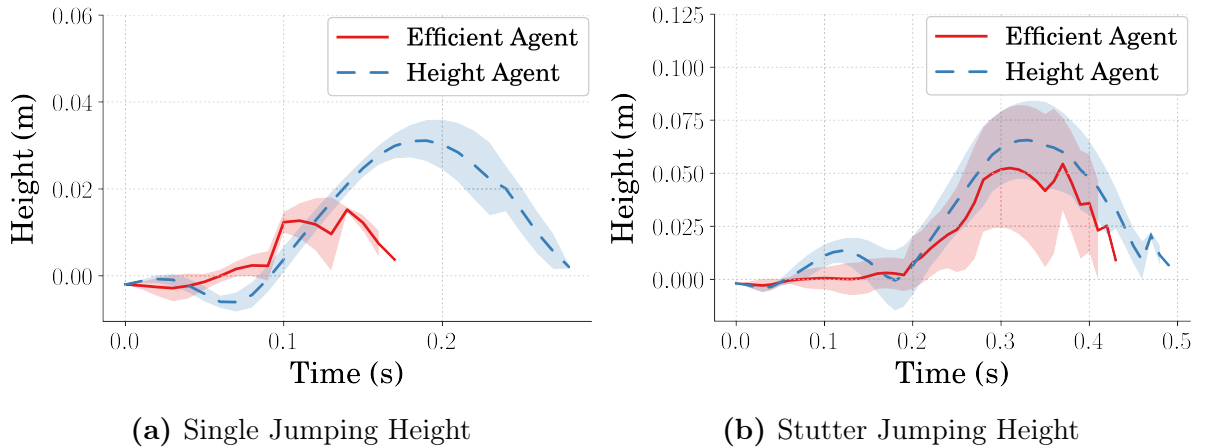


**Figure 10.** Average and Standard Deviation Heights of monopode

of leaving the ground, then recompressing for a much higher jump. Summing up the single jumping commands, the efficient strategy trained controllers that jumped the monopode 104.53% lower than the high jumping strategy.

Figure 10b compares the jumping performance of the efficient and height strategies for the stutter jumping command. At first glance, they differ, but less drastically than the single jumping case. The likeness of the input command shapes propagate and the resulting jumping shapes share similar in form. The large differences seen in the stutter jumping shapes are similar those of the inputs that create them, in that they differ mostly regarding the magnitudes. Summing up the stutter jumping command, the efficient strategy resulted in a jumping command that jumped 20.69% lower than the high jumping strategy.

In both the single and stutter jumping cases, the upward acceleration from efficient controllers toward the end of the command can be seen in that the position of the monopode creates a psuedo plato. Additionally, regarding variance, the single jumping controllers seems to produce jumping shapes with similar levels of variance. As for the stutter jumping case, though similar in high levels of input variance, the jumping height variance for the efficient controllers is noticeably higher than that of the height controller.

**2.5.3 Height Reached vs. Power Used.** Height reached versus power consumed data, for both the single jumping and stutter jumping cases is shown in Figure 11. It is firstly apparent that in both the single and stutter jumping cases, the efficient controllers utilize less power and therefore suffer regarding jump height. This matches what was seen in the previous sections regarding input commands and jumping shapes. In the single jumping case, shown in Figure 11a, there is an apparent separation between the two controller types where the height controllers are mostly clustered in the upper-right part of the dataset. On average, for the single jumping

command type, the efficient jumping strategy learned jumping commands that were 126.27% more efficient. As for the stutter jumping case, show in Figure 11b, the difference is less obvious though still present. The variance of the two controller types, being quite high, matches what is seen in the previous sections and results in more mixing of the data. On average, for the stutter jumping command type, the efficient strategy learned commands that were 101.45% more efficient.

## 2.6 Optimal Performance of Network Controller

**2.6.1 Input Commands.** Taking the best of the fifty different controllers trained for both the single and stutter jumping cases and comparing the efficient and

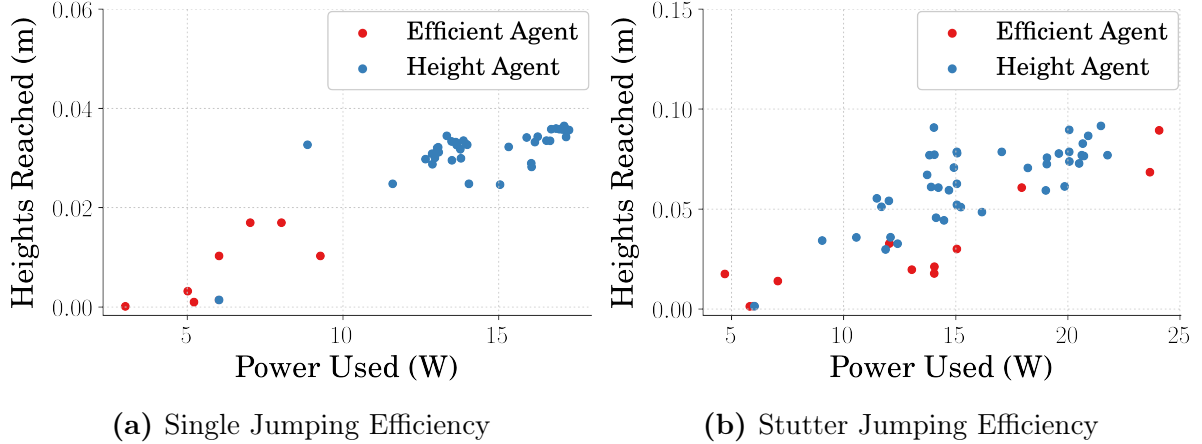


**Figure 11.** Height Reached vs Power Consumed of monopode

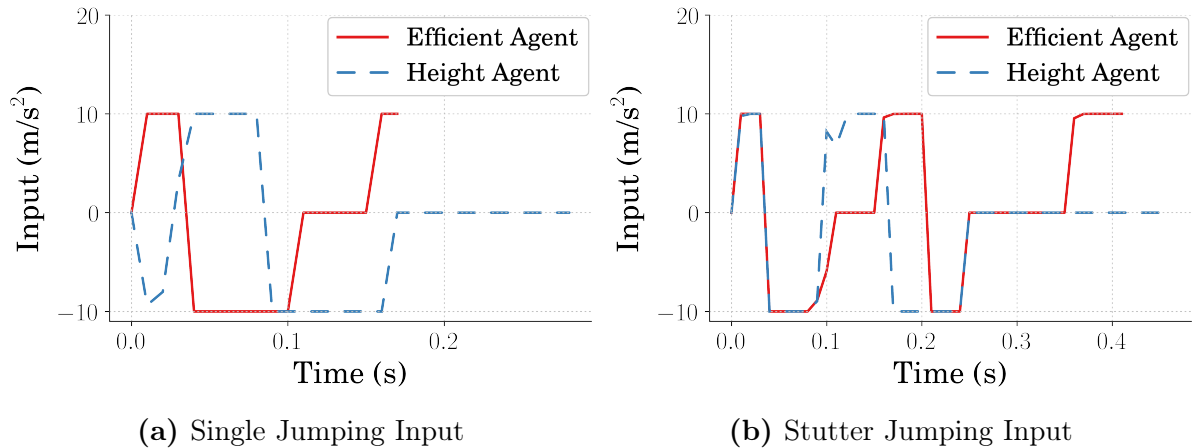


**Figure 12.** Optimal Inputs to monopode

height controller's performance can show what is possible with a properly defined RL problem. Figure 12, shows the differences in the input commands generated when selecting the highest performing controller in terms of reward received. At first glance, it can be seen that there are less differences between the the efficient and height controllers in comparison to the average results from Section 2.5. A major similarity being that magnitudes are similar across all cases such that the controllers utilize the actuator's maximum acceleration. Looking at Figure 12a, which compares the efficient and height controllers for the single jumping input, the major difference are of course the timing and direction of the command. This is similar to the average performance evaluation, from Section 2.5.1, in that the efficient controller does not take advantage of the slight decompression of the spring before the monopode leaves the ground. Because of this, the efficient controller learns a different timing for a single jump. As for the stutter jumping case, shown in Figure 12b, the differences between the efficient and height controller is less drastic. The initial timing is largely the same as both controller types learn to utilize the decompression of the spring. The differences begin when decompressing the spring a second time and completing the first jump. The efficient controller learns a command similar in form to a bang-coast-bang command, where in contrast the height controller learns a command similar to that of a bang-bang shaped input.

**2.6.2 Jumping Height Performance.** In line with the previous section, it is of interest to evaluate the jumping performance curves of the best controllers trained. Figure 13 displays the jumping performance for both jump types as well as both controller types when utilizing the inputs shown in Section 2.6.1. These curves validate what was shown in the previous section and display that the efficient controllers do not generate commands that jump the monopode as high. Figure 13a, which compares the efficient and height controllers for the single jump, verifies that the efficient controller

does not learn to utilize the slack in the spring. In Figure 13b, it can be seen that when utilizing a command more similar in form to a bang-coast-bang command, like the efficient controller learned, the timing of the jump sequence is shifted and the resulting final height is less than the height controller who's command is more similar to a bang-bang shaped command.

## 2.7 Conclusion

Two different controller types where trained to generate two different jumping commands for the simplified monopode jumping system described in Section 2.1. The first type of controller was one that would command the monopode system to jump high where the reward was based on nothing other than system height. The second type of controller was one which controlled the monopode to jump high but at the cost of power consumed, such that high jumps that consumed high amount of power were less desirable than high jumps that consumed less power. It has been shown that the rewards past to RL algorithms that are training controllers can be manipulated so that the learned input commands take advantage of the spring/damper that exists within the monopode jumping system. Furthermore, the timing of the commands, the input magnitude and direction are all affected when defining a reward strategy that

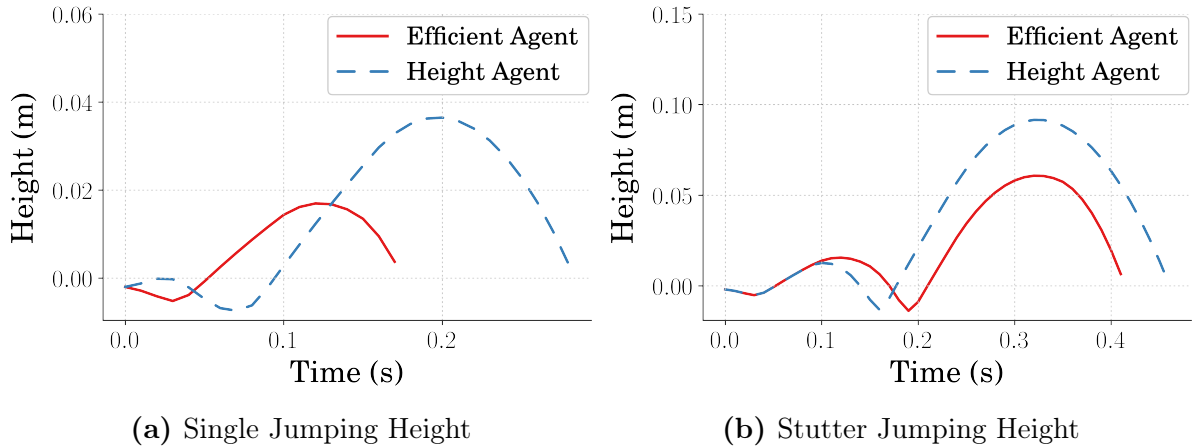


**Figure 13.** Optimal Heights of monopode

seeks to increase power efficiency. When considering the average performance of the different control strategies, for both the single and stutter jumping cases, the heights reached were less for the efficient strategies. However, they were significantly more efficient, particularly when scaling the complexity of the command from the single jump to the stutter jump. It should be concluded then, that RL might serve as a useful method for defining control strategies for flexible-legged jumping systems, particularly when energy efficiency is of interest. Additionally, when considering more complex control strategies, which might be difficult to define efficiently, RL might serve as a useful method for effective efficient strategies.

### III Using Input Shaping to Validate RL Controller

In utilizing RL to define a control strategy for a robotic system, the resulting commands sent to the system are often described as optimal, or at least approaching optimal. They are described as such due to the nature of RL problems in that the techniques used to learn a policy are optimization theory based so the policy being trained is one that is approaching an optimal solution in regards to the reward defined. Interpreting the commands claimed to be optimal, in the context of control theory, is an important part of utilizing RL for defining control strategies for robotic systems however. In the case of a flexible jumping robot, where the command is to jump the system as high as possible or as efficient as possible, are the commands generated truly approaching an optimal solution? Methods such as input shaping, having been shown to be an effective method for defining optimal control strategies for flexible jumping systems, can be used to evaluate the commands generated by the RL generated policies [39].

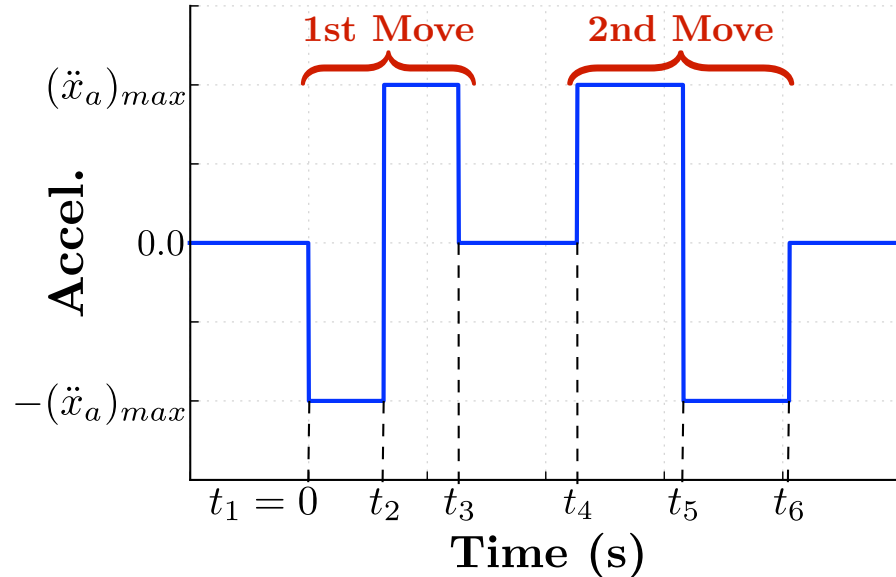


**Figure 14.** Jumping Command

### 3.1 Input Shaping Controller Input

Bang-bang based jumping commands like the one shown in Figure 14 are likely to result in a maximized jump height [39]. For these command types, regarding the

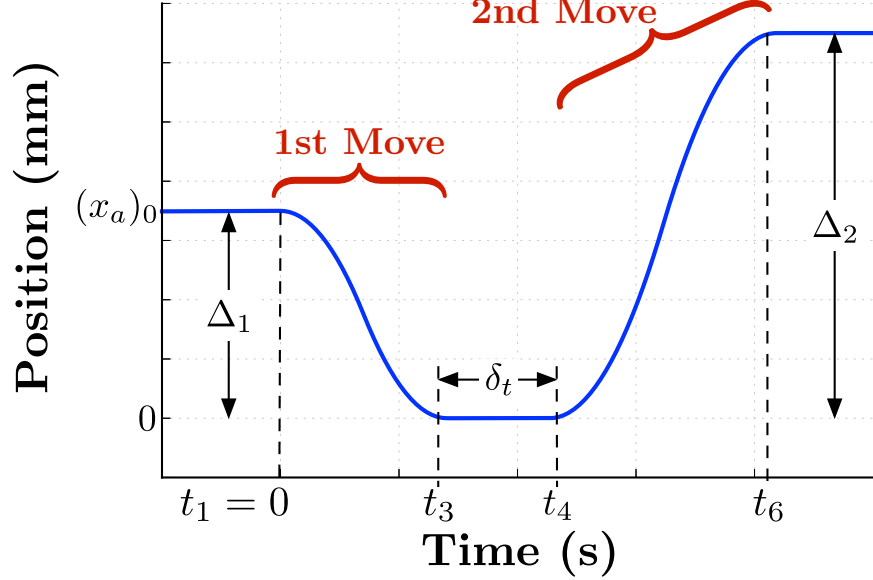


**Figure 15.** Resulting Actuator Motion

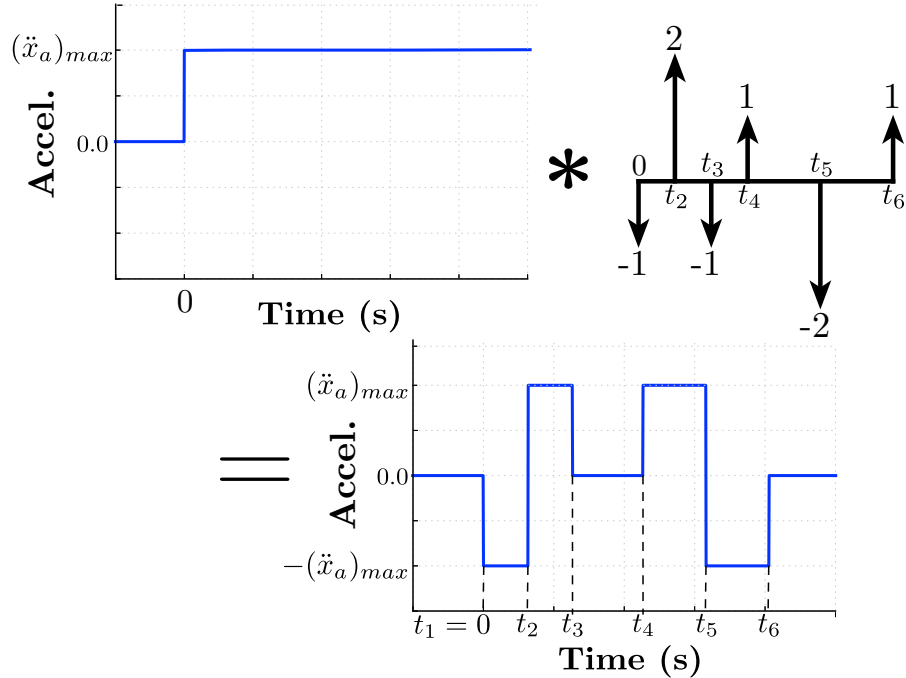


**Figure 16.** Decomposition of the Jump Command into a Step Convolved with an Impulse Sequence

monopode jumping system, the actuator mass travels at maximum acceleration within its allowable range, pauses, then accelerates in the opposite direction. Commands designed to complete this motion are bang-bang in each direction, with a selectable delay between them. The resulting motion of the actuator along was rod is shown in Figure 15. Starting from an initial position,  $x_{a_0}$ , the actuator moves through a motion of stroke length  $\Delta_1$ , pauses there for  $\delta_t$ , then moves a distance  $\Delta_2$  during the second portion of the acceleration input.

This bang-bang-based profile can be represented as a step command convolved with a series of impulses, as was shown in Figure 16 [40]. Using this decomposition, input-shaping principles and tools can be used to design the impulse sequence [41, 42]. For the bang-bang-based jumping command, the amplitudes of the resulting impulse sequence are fixed,  $A_i = [-1, 2, -1, 1, -2, 1]$ . The impulse times,  $t_i$ , can be varied and optimal selection of them can lead to a maximized jump height of the monopode system [39]. Commands of this form will often result in a stutter jump like what was shown in Figure 7b of Chapter 2, where the small initial jump allows the system to compress the spring to store energy to be used in the final jump.

### 3.2 RL Controller Input

Discussion and figures from the inputs defined by the RL algorithms for the monopode system.

...

Lets have a chat and discuss what we want to do here.

### 3.3 Conclusion

Discuss the results.

## IV Mechanical Design of a the Monopode Jumping System

Often it is the goal of a controls engineer to design a controller to accommodate and manipulate systems according to the system description provided. However, research has been conducted showing the value of studying the manipulation of mechanical design parameters in order to achieve a desired system behavior [16]. In this chapter, reinforcement learning is shown to be useful as a tool to learn mechanical designs given a predefined system controller for the monopode jumping system. RL has been shown to be an effective strategy for finding optimal concurrent designs for many different types of systems [18, 43, 44]. It has even shown it's ability to define designs that are successfully deployed on physical hardware [17]. It is comparable to work where evolutionary type algorithms are deployed to optimize physical parameters of systems for improved energy efficiency [45, 46]. Here, RL is used to define an optimal design for the monopode jumping system described in Chapter 2.

### 4.1 Learning a Mechanical Design

Section 1.4 describes the common deployment methodology of an RL problem where defining a control policy for a robotic system is often the primary goal. In this Chapter, rather than finding a control policy for a defined robotic system, RL is deployed to find a mechanical design for a defined control input. To do this, the general methods in setting up the problem have to change.

The RL problem here is similar to the common use case in that the algorithm utilizes the same information types to optimize a design, such as the state of the environment and the reward. The algorithm's interaction with the environment is drastically different however. The action space, instead of being a command type input, is a range of design choices for a set of parameters within a simulation of a system. Applying these actions within the environment, rather than changing the state of a robotic system from state  $s$  to  $s'$ , instead simulates a system within the environment

from time  $t = 0$  to time  $T$  using a predefined control input. Because of this, the state saved as a transition is a matrix of states rather than a single vector state. The reward does not differ greatly in that it is based on the state of the system. A difference being that the information stored in a single state transition is much greater so the reward can be defined to utilize all the information.

For the work presented in this Chapter, the predefined control input used to simulate the system within the environment at each step was an optimized controller generated using the input shaping techniques discussed in Section 3.1. Having been shown to be a useful technique for generating optimal control strategies, it was of interest to evaluate if an optimal mechanical design could be found to accompany the input.

## 4.2 Environment Definition

To allow the agent to find a mechanical design, a reinforcement learning environment conforming to the OpenAI Gym standard [36] was created. The monopode model described in Chapter 2 was used as the simulation, and the fixed controller input was based on the work described in Section 3.1. The mechanical parameters the agent was tasked with optimizing were the spring constant and the damping ratio of the monopode system. At each episode during training, the agent selected a set of design parameters from a distribution of available designs. The actions applied,  $\mathcal{A}$ , and transitions saved,  $\mathcal{S}$ , from the environment were defined as follows:

$$\mathcal{A} = \{\{a_\alpha \in \mathbb{R} : [-0.9\alpha, 0.9\alpha]\}, \{a_\zeta \in \mathbb{R} : [-0.9\zeta, 0.9\zeta]\}\} \quad (16)$$

$$\mathcal{S} = \left\{ \sum_{t=0}^{t_f} x_t, \sum_{t=0}^{t_f} \dot{x}_t, \sum_{t=0}^{t_f} x_{at}, \sum_{t=0}^{t_f} \dot{x}_{at} \right\} \quad (17)$$

where  $\alpha$  and  $\zeta$  are the nominal spring constant and damping ratio of the monopode, respectively;  $x_t$  and  $\dot{x}_t$  are the monopode's rod height and velocity steps, and  $x_{at}$  and

$\dot{x}_{at}$  are the monopode's actuator position and velocity steps, all captured during simulation.

### 4.3 Rewards for Learning Designs

The RL algorithm was utilized to find designs for two different reward cases. Time series data was captured during the simulation phase of training and was used to evaluate the designs performance through these rewards. The first reward case used was:

$$R_1 = \left( \sum_{t=0}^{t_f} x_t \right)_{max} \quad (18)$$

where  $x_t$  was the monopode's rod height at each step during simulation. The goal of the first reward was to find a design that would cause the monopode to jump as high as possible.

The reward for the second case was:

$$R_2 = \frac{1}{\frac{|R_1 - x_s|}{x_s} + 1} \quad (19)$$

where  $x_s$  was the desired jump height, which was set to 0.01 m. The second case was utilized to test RL's ability to find a design that minimized the error between the maximum height reached and the desired maximum height to reach.

### 4.4 Design Space Variations

Figures 17 and 18 represent the heights the monopode could reach for two different design spaces. The design space provided for the first case, shown in Figure 17, represents a space where the allowable damping ratio was limited to a fairly narrow range. This limits the solution space, making it less likely that the agent will settle to a locally optimal value. The design space provided for the second case, shown in Figure 18, represents a space where a wider range of damping ratios are allowed. This wider range of possible values makes it more likely that the agent will settle to a local maxima.

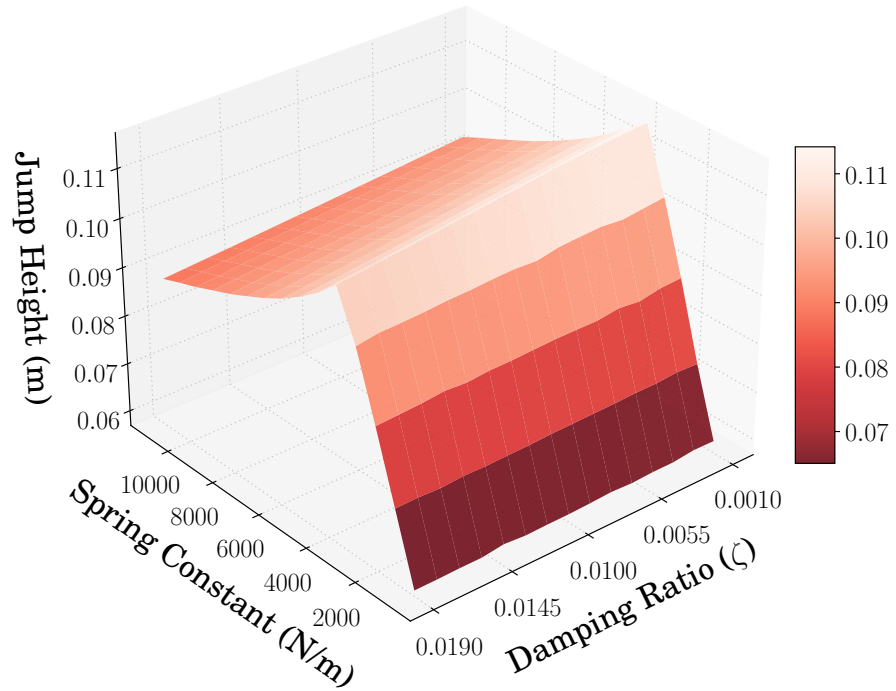


**Figure 17.** Jumping Performance of Narrow Design Space

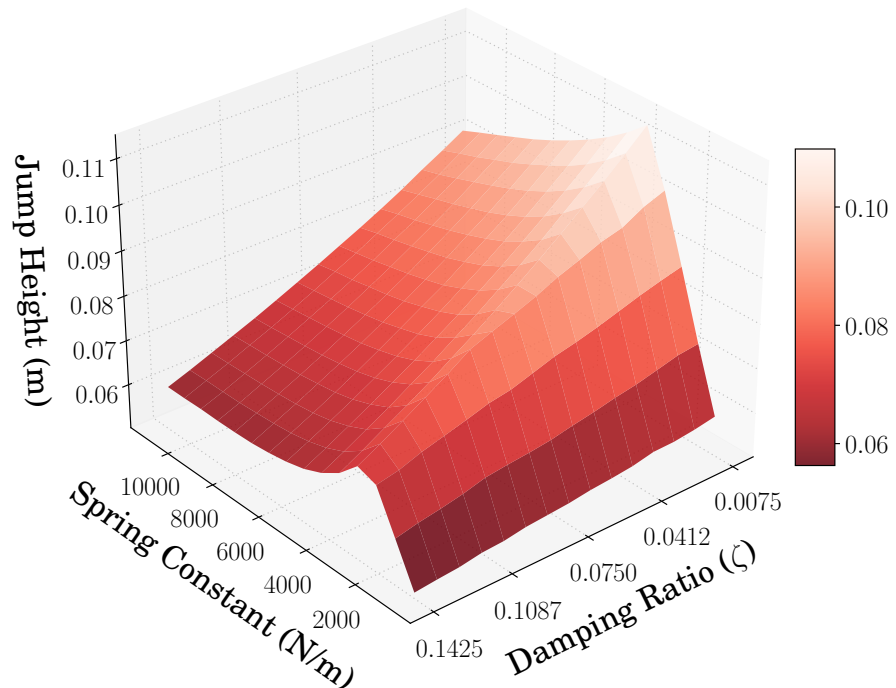


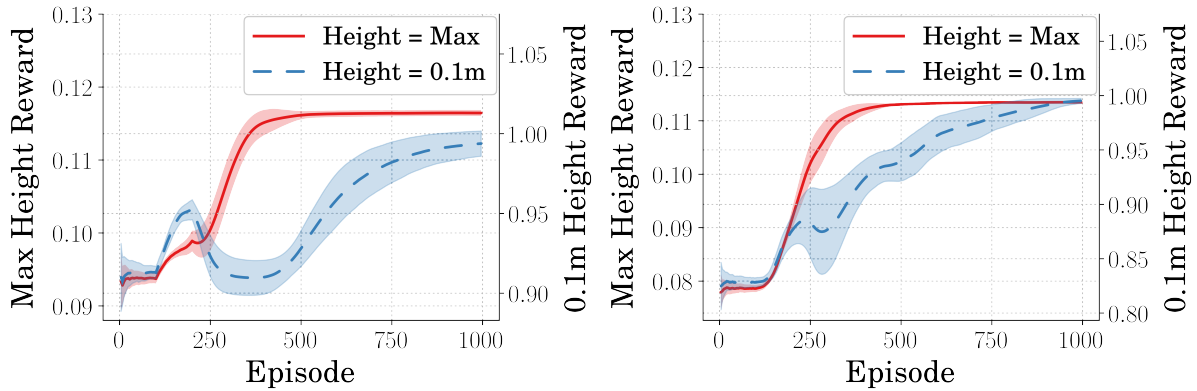
**Figure 18.** Jumping Performance of Broad Design Space

## 4.5 Deploying TD3

The training hyperparameters were selected based on TD3’s author recommendations and StableBaselines3 [27] experimental findings and are displayed in Table 3. All of the hyperparameters, with the exception of the rollout (Learning Starts) and the replay buffer, were set according to Stable Baselines3 standards. The rollout setting was defined such that the agent could search the design space at random, filling the replay buffer with enough experience to prevent the agent from converging to a design space that was not optimal. The replay buffer was sized proportional to the

**Table 3.** TD3 Training Hyperparameters

Hyperparameter	Value
Learning Rate, $\alpha$	0.001
Learning Starts	100 Steps
Batch Size	100 Transitions
Tau, $\tau$	0.005
Gamma, $\gamma$	0.99
Training Frequency	1:Episode
Gradient Steps	$\propto$ Training Frequency
Action Noise, $\epsilon$	None
Policy Delay	1 : 2 Q-Function Updates
Target Policy Noise, $\epsilon$	0.2
Target Policy Clip, $c$	0.5
Seed	100 Random Seeds



(a) Reward vs. Episode: Narrow Design Space (b) Reward vs. Episode: Wide Design Space

**Figure 19.** Reward vs. Episode for Learning Mechanical Design

number of training steps due to system memory constraints.

The average rewards for both the narrow and the wide design space agents are shown in Figure 19. They represent the agents learning a converging solution to the problem of finding optimal design parameters. Looking at Figure 19a, it is apparent that given a more narrow design space, both the high and the specified jumping agents were still able to learn a converging solution. It can also be observed that there exists more variance for the specified height agent type compared to the height agents. Looking at Figure 19b, it is also apparent that the agents given a broader design space where both able to learn a converging design solution. Though given more designs to choose from, it appears the specified height agents are taking longer to search the design space, and towards the end, finding a designs with less variance.

## 4.6 Jumping Performance

**4.6.1 Narrow Design Space.** Figure 20 shows the height achieved by the learned designs for the agents given the narrow range of possible damping ratio values. For the agents learning designs to maximize jump height, Figure 20 can be compared

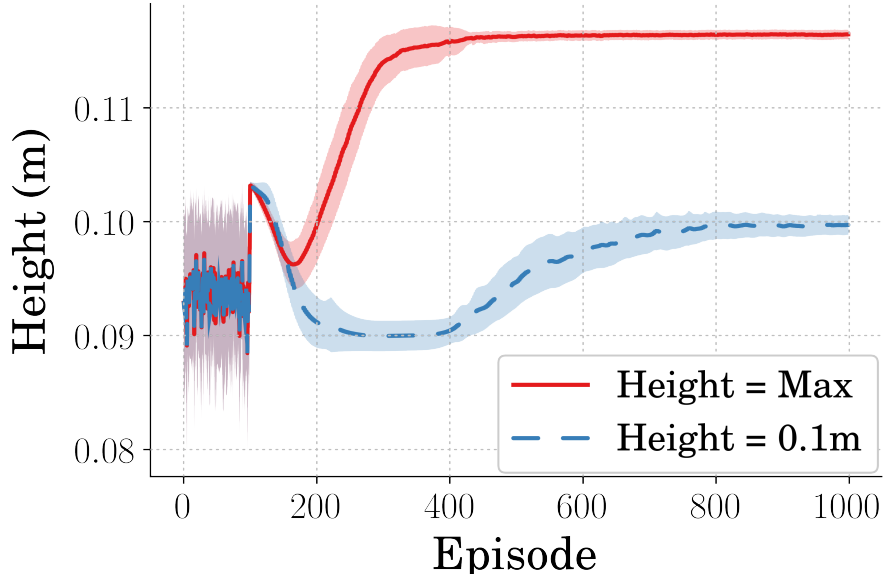


**Figure 20.** Height Reached During Training

with Figure 17 showing that the agent learned a design nearing one which would achieve maximum performance. Additionally, looking at the agents learning designs to jump to the specified 0.1 m, the designs learned accomplish this with slightly more variance than that of the maximum height case.

The average and standard deviation of the spring constant and damping ratio

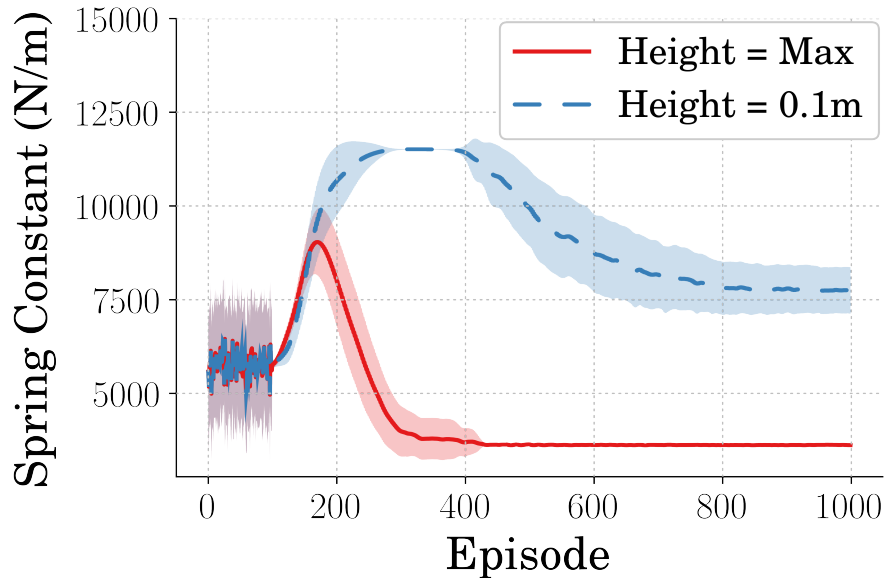


**Figure 21.** Spring Constant Selected During Training

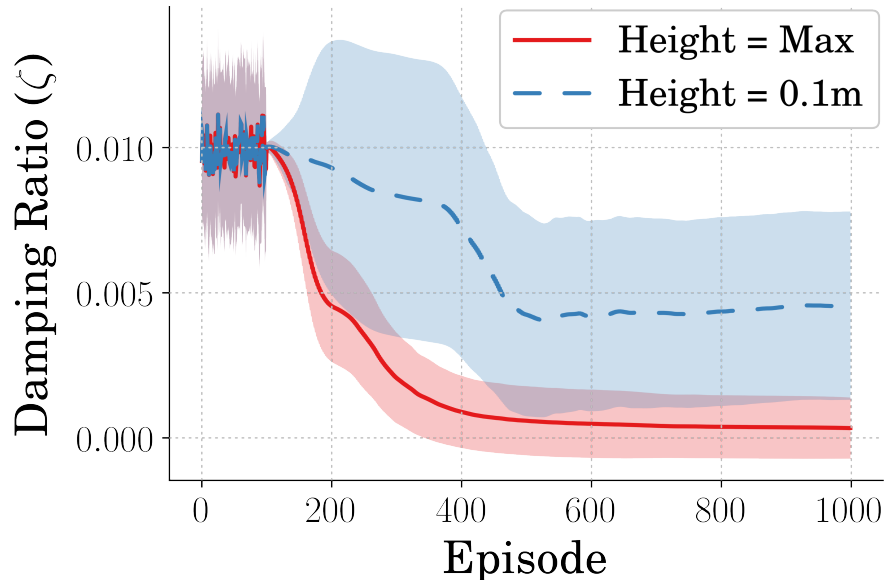


**Figure 22.** Damping Ratio Selected During Training

design parameters the agents selected during training are shown in Figs. 21 and 22. These plots represent the learning curves for the agents learning design parameters to maximize jump height and the agents learning design parameters to jump to 0.01 m. There is a high variance in both the spring constant and the damping ratio found for the agents that learned designs to jump to a specified height. The agents which were learning designs which maximized height found designs with very little variance in terms of spring constant and significantly less variances in terms of damping ratio.

**4.6.2 Wide Design Space.** Figure 23 shows the height achieved by the learned designs for the agents given a wider range of damping ratios. For the agents learning designs to maximize jump height, Figure 23 can be compared with Figure 18 showing that the agents learned a design nearing one which would achieve maximum performance. Additionally, looking at the agents learning designs to jump to the specified 0.1 m, the designs learned accomplish this, only with slightly more variance than what is seen in the maximum height agents.

The average and standard deviation of the spring constant and damping ratio

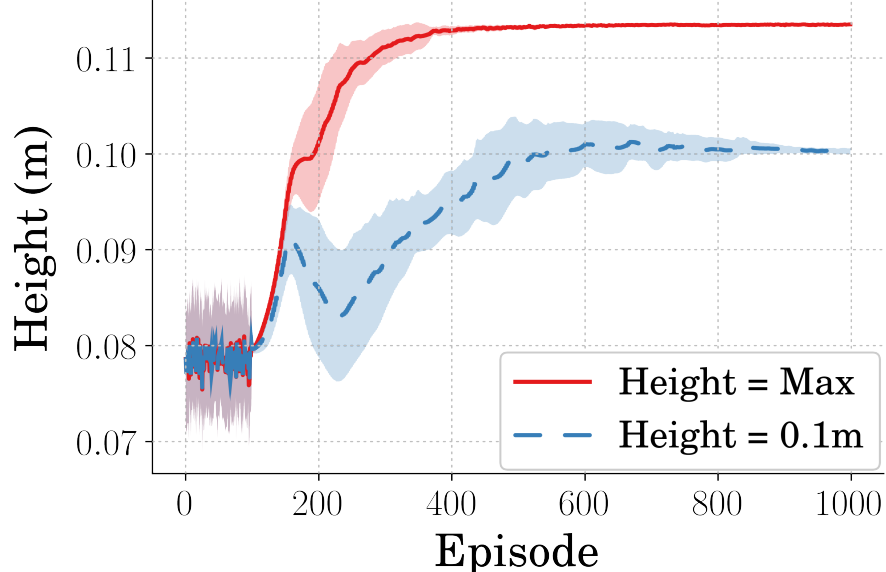


**Figure 23.** Height Reached During Training

design parameters the agents selected during training are shown in Figures 24 and 25. For the agents that learned designs to jump to a specified height, it can be seen that there is a high variance in spring constant throughout training. However, the majority of agents converge to a specific design, lowering the variance. The same can be seen in the damping ratio; however, the variance is mitigated significantly earlier in training.

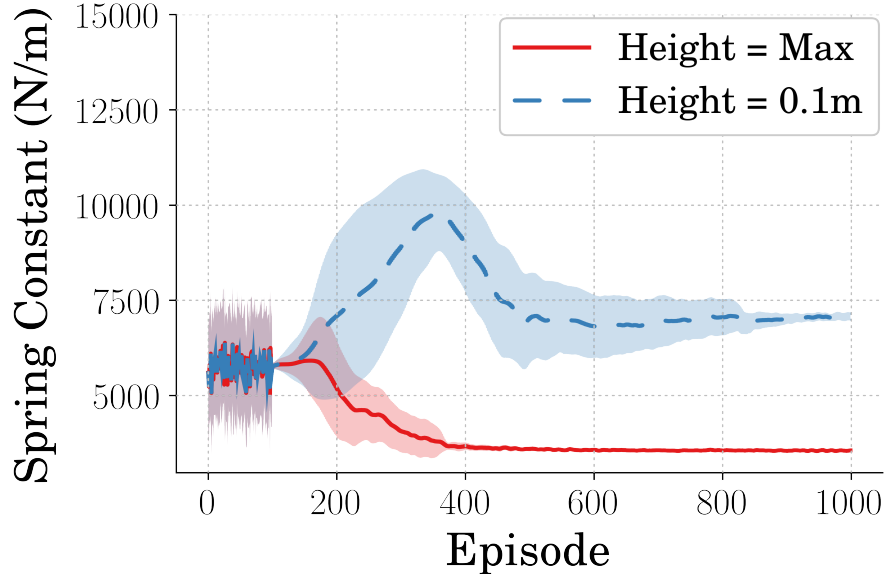


**Figure 24.** Spring Constant Selected During Training

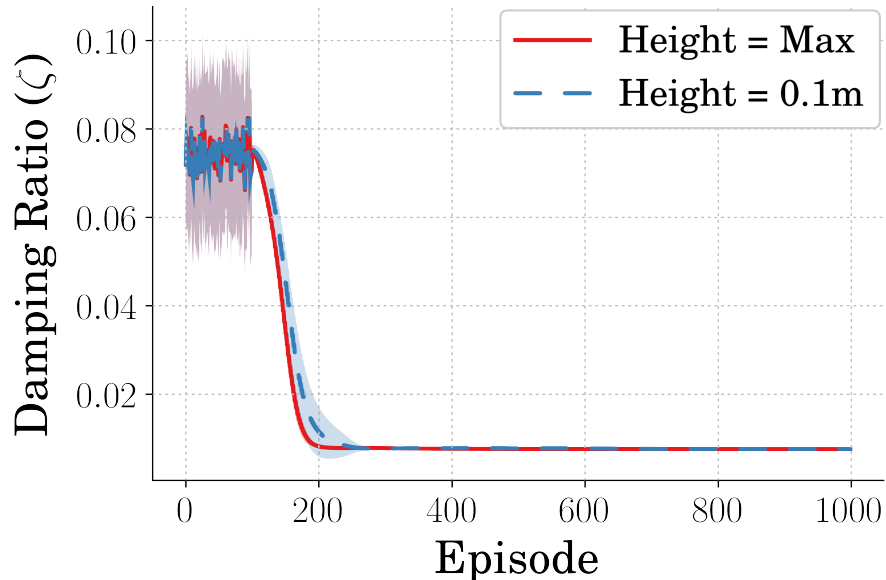


**Figure 25.** Damping Ratio Selected During Training

The agents which were learning designs that maximized height found them with very little variance in terms of spring constant and damping ratio.

**4.6.3 Average Design Performance.** The final mean and standard deviation of the design parameters for the two different cases are presented in Table 4. Figure 26 shows the jumping performance of the mean designs learned for both cases tested. The agents tasked with finding designs to jump to the specified 0.1 m, did so with minimal error. The difference seen in maximum height reached between the two

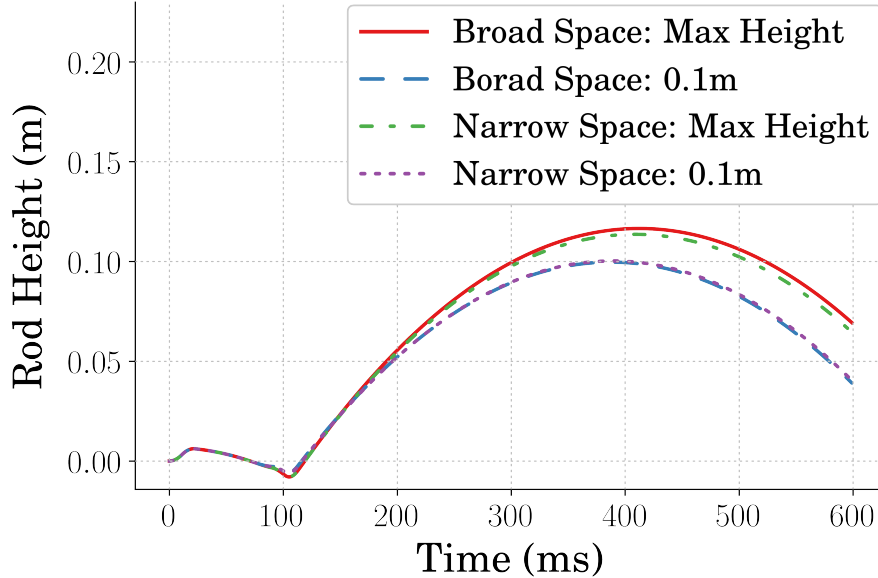


**Figure 26.** Height vs Time of Average Optimal Designs

**Table 4.** Learned Design Parameters

Training Case	Design Parameter	Mean	STD
Narrow Design Space	Max Height Spring Constant	3.62e03	3.82e01
	Max Height Damping Ratio	3.37e-04	2.11e-03
	Specified Height Spring Constant	7.74e03	1.24e03
	Specified Height Damping Ratio	4.55e-03	6.49e-03
Broad Design Space	Max Height Spring Constant	3.55e03	4.86e01
	Max Height Damping Ratio	7.53e-03	8.86e-06
	Specified Height Spring Constant	7.07e03	2.16e02
	Specified Height Damping Ratio	7.54e-03	3.27e-05

cases represents the difference in the damping ratio design space the agents had access to. The peak heights achieved can be compared again to Figures 17 and 18 to show that the agents learned designs nearing those achieving maximum performance.

#### 4.7 Conclusion

The monopode model was used in conjunction with a predetermined control input to determine if a reinforcement learning algorithm (TD3) could be used to find optimal performing design parameters regarding jumping performance. This work was done in part to determine if reinforcement learning could be used as the mechanical design learner for an intelligent concurrent design algorithm. It was shown that when providing an agent with a design space that was smaller in size, the agents performed well in finding design parameters which met the performance constraints. The designs found were high in design variance, however. It was additionally shown that when provided with larger design space, the agents excelled at finding design parameters which were lower in design variance but still met the design constraints. It should be concluded ultimately that utilizing an RL algorithm, such as TD3, for the mechanical design aspect of a concurrent design method, is a viable solution.

## V Concurrent Design of the Monopode System

Finding a control architecture for a mechanically defined system is often the the workflow for generating a controlled robotic system. However, the mechanical system is not always a simple one and generating a controller for it may require a more complex workflow. It is of interest as well to allow the mechanical parameters of the system, and therefore the system description, to be fluid, allowing for a more optimal mesh between controller and system. Designing the system and control input in unison has been researched and is often referred to as concurrent design. This strategy has been used to develop better performing mechatronics systems [16]. More recent work has used advanced methods such as evolutionary strategies to define robot design parameters [45]. In addition to evolutionary strategies, reinforcement learning has been shown to be a viable solution for concurrent design of 2D simulated locomotive systems [44]. This is further shown to be a viable method by demonstrating more complex morphology modifications in 3D reaching and locomotive tasks [18]. However, these techniques have not yet been applied to flexible systems for locomotive tasks. In this Chapter, a novel definition of a concurrent design architecture is purposed to find an optimal design and controller for the monopode jumping system defined in Chapter 2.

### 5.1 Concurrent Design Architecture

To define a concurrent design process utilizing RL, an algorithm is proposed which utilizes two instances of the TD3 algorithm creating an inner and an outer loop. The first instance, being responsible for learning the control policy, will be instantiated in a similar fashion to the what is seen in Chapter 2. It is the outer loop of the concurrent design process. The second instance, being responsible for learning the mechanical design, is instantiated within the outer loop and in a similar fashion to what is seen in Chapter 4. The second instance is the inner loop of the concurrent design

process. A key aspect of the inner loop instantiation is that rather than using a pre-defined control input, like what was shown in Chapter 4, the simulation will be using the input being trained by the outer loop instantiation. The algorithm is presented in Appendix 6 in greater detail.

## 5.2 Mechanical Design Update

**5.2.1 Discrete vs. Continuous.** As is further discussed in Appendix 6, there are two different methods for implementing the inner loop of the concurrent design algorithm. The first is called the *discrete* method, where at each environment design update, the model learning the design is instantiated fresh and learns a design from scratch. The second method is called *continuous*, where at each environment update the model learning the design is saved and reloaded so that the model that is learning a design is the same over the course of the controller model training.

**5.2.2 Averaging  $n$  Design Policies.** In Chapter 4, average designs found from 50 different policies are shown, and it can be seen that design choice can vary between policies depending on factors such as the reward the policy receives and the design space limits. To replicate these results and to ensure that the mechanical design inner loop did not suffer from a single policy finding a locally optimal design,  $n$  number of design policies were instantiated at each design update. The average of the  $n$  designs found was used to update the environment within the outer loop. This methodology was applied to both the discrete and the continuous methods of mechanical design update. In this work,  $n$  was set as 10 as it proved to resolve one of the policies finding a locally optimal design.

**5.2.3 Differing Reward Types.** Depending on the reward passed to the design update inner loop, the performance of the control policy may immediately increase or decrease when the design is updated. For example, if the rewards for both

inner and outer loops reward the same metric, the control policy within the outer loop should see an increase in performance after a design update. If however, the rewards for the inner and outer loops differ, where the outer loop might reward height for example and the inner rewards efficiency, the control policy may experience an immediate decrease in performance after a design update. Utilizing differing rewards might serve as a tool to generate designs where, as suggested, the control policy is defined to accomplish a task and the design is optimized to allow the control policy to do that task efficiently.

**5.2.4 Design Update Rate.** When the inner loop makes an update to the environment that the policy within the outer loop is being trained on, the policy should see an immediate performance change. These step like changes are likely to result in a policy learning less data efficiently. Because of this, a new hyperparameter is introduced being the rate at which the design is updated. As is shown in Appendix 6, the design is updated in line with the control policy only not at the same rate. It is suggested that for this architecture the design is updated every  $n$  policy updates where  $n$  depends on the complexity of the control policy being trained. For more complex control policies, where the learning process might require more environment interactions to learn,  $n$  should be set to a higher value so that the control policy can learn a design without the added difficulty dynamic environment design parameters. In this work,  $n$  is set to 100.

### 5.3 Environment Definition

**5.3.1 Learning the Controller.** The outer loop of the concurrent design architecture was defined similar to what was shown in Chapter 2, where a traditional RL environment aligning with the standards set by OpenAI for a Gym environment was created [36]. The monopode, also described in Section 2.1, was used to define the environment and evaluate the methods discussed in this Chapter. The action and

observation spaces were defined, respectively, as follows:

$$\mathcal{A} = [\ddot{x}_{a_t}] \quad (20)$$

$$\mathcal{S} = [x_{a_t}, \dot{x}_{a_t}, x_t, \dot{x}_t] \quad (21)$$

where  $x_t$ ,  $\dot{x}_t$  were the monopode's position and velocity at time  $t$ , and  $x_{a_t}$ ,  $\dot{x}_{a_t}$  and  $\ddot{x}_{a_t}$  were the actuator's position, velocity and acceleration, respectively.

Differing from the evaluation completed in Chapter 2, only the stutter jumping command was evaluated. Therefore the stopping conditions for the environment were either the monopode completing two jumps or the time step limit. For this work, the time step limit was set to 400 steps at 0.01 seconds per step. Additional information regarding the stutter jump command are further discussed in Section 2.1. Furthermore, the values of the monopode's nominal constants are shown in Table 1 within Section 2.1.

**5.3.2 Learning the Design.** To allow the inner loop RL algorithm to find a mechanical design within the outer control loop, a second reinforcement learning environment was defined, again conforming to the OpenAI Gym standard [36], in a similar fashion to what was discussed in Chapter 4. Differing from Chapter 4 however, the control input, rather than being fixed, is captured from the outer loop and used to evaluate the performance of different design choices. The mechanical parameters the algorithm was tasked with optimizing were the spring constant and the damping ratio of the monopode jumping system.

At each episode during training, the algorithm's policy selected a set of design parameters from a distribution of predefined parameter ranges. The actions applied,  $\mathcal{A}$ , and transitions saved,  $\mathcal{S}$ , from the environment were defined as follows:

$$\mathcal{A} = \{ \{a_\alpha \in \mathbb{R} : [-0.9\alpha, 0.9\alpha]\}, \{a_\zeta \in \mathbb{R} : [0, 0.01]\} \} \quad (22)$$

$$\mathcal{S} = \left\{ \sum_{t=0}^{t_f} x_t, \sum_{t=0}^{t_f} \dot{x}_t, \sum_{t=0}^{t_f} x_{a_t}, \sum_{t=0}^{t_f} \dot{x}_{a_t} \right\} \quad (23)$$

where  $\alpha$  is the nominal spring constant the monopode,  $x_t$  and  $\dot{x}_t$  are the monopode's rod height and velocity steps, and  $x_{at}$  and  $\dot{x}_{at}$  are the monopode's actuator position and velocity steps, all captured during simulation. The nominal values of the constants are shown in Table 1 within Section 2.1.

## 5.4 Deploying the Algorithm

As is discussed in Section 5.1, an inner and outer instantiation of the TD3 algorithm are generated to create the concurrent design architecture. Similar to what was practiced in previous Chapters, multiple instances of the algorithm were run to evaluate the ability of the architecture to perform with different network initializations. In this work, 10 total instances were evaluated so that average performance data could be collected. This proved to be an effective amount needed to evaluate variances seen in performance.

The outer loop was instantiated in a similar fashion as to what was discussed in Chapter 2, only the number of total training steps was increased from 500k to 750k. This was done as the control policy was anticipated to be more difficult to learn given the environments parameters would be changing due to the inner loop. The training

**Table 5.** Outer Loop TD3 Training Hyperparameters

Hyperparameter	Value
Learning Rate, $\alpha$	0.001
Learning Starts	1000 Steps
Batch Size	100 Transitions
Tau, $\tau$	0.005
Gamma, $\gamma$	0.99
Training Frequency	1:Episode
Gradient Steps	$\propto$ Training Frequency
Action Noise, $\epsilon$	None
Policy Delay	1 : 2 Q-Function Updates
Target Policy Noise, $\epsilon$	0.2
Target Policy Clip, $c$	0.5
Seed	10 Random Seeds

hyperparameters used for the outer loop instantiation of the TD3 algorithm are presented in Table 5.

The inner loop, similar to the outer, was instantiated in a similar fashion to what is shown in Chapter 4. This instantiation of the TD3 algorithm is created within the outer instantiation of the TD3 algorithm, using the policy being trained within the outer loop to optimize the environment used in the outer loop. The hyperparameters used for each of the 10 instantiations of the inner loop TD3 algorithm are presented in Table 6.

## 5.5 Mechanical Designs

...  
I am re making some of this data training for longer. Training for shorter than the less complex work seems counterintuitive.

Of the different approaches discussed, the one highlighted here is a discrete method where the design parameters were updated every 100 control policy updates. Figure 27 displays the average learning of the designs during the training of the control policy for both the efficient and high jumping control types. This data was captured at

**Table 6.** TD3 Training Hyperparameters

Hyperparameter	Value
Learning Rate, $\alpha$	0.001
Learning Starts	100 Steps
Batch Size	100 Transitions
Tau, $\tau$	0.005
Gamma, $\gamma$	0.99
Training Frequency	1:Episode
Gradient Steps	$\propto$ Training Frequency
Action Noise, $\epsilon$	None
Policy Delay	1 : 2 Q-Function Updates
Target Policy Noise, $\epsilon$	0.2
Target Policy Clip, $c$	0.5
Seed	10 Random Seeds

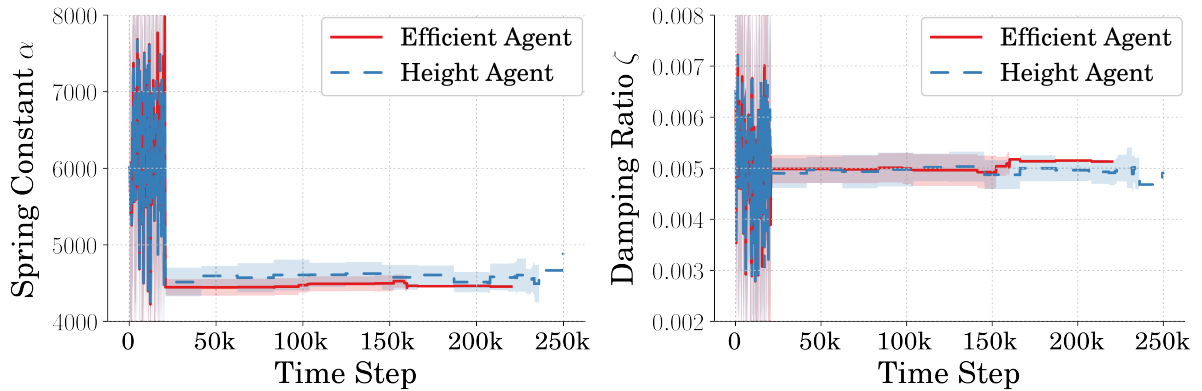
every 500 control policy update interval, after the environment's parameters were updated per the learned design. It is apparent that the design policy can learn a design early in training, even utilizing a loosely defined control policy. It is also apparent that the design learned early in the training process is one that is close to optimal for the control policy even after the control policy is better defined. Figure 27a showing the learning of the spring constant shows that the efficient controller types learn a lower value to increase efficiency. Figure 27b being the learning of the damping ratio, shows little difference between the two control types.

## 5.6 Controller Performance

...  
I am re making some of this data training for longer. Training for shorter than the less complex work seems counterintuitive.

Ten different control policies were trained and each of them was trained to be optimal with a specific design. Therefore, to evaluate the average performance of the concurrent design method discussed in this Chapter, each of the policies was evaluated on its respective optimal design and the performance of them were averaged.

Figure 28 shows the average input learned from the control policies for the efficient and high jumping control types. Similar to what was seen in Chapter 2, it is



(a) Spring Constant Selected During Training (b) Damping Ratio Selected During Training

**Figure 27.** Designs Learned Using Update Rate = 1:500 Control Policy Updates

apparent that there are distinct differences in the control techniques from the efficient and high controllers. Like what was discovered within the single jump command from Chapter 2, the efficient controller type learns a policy that in its first acceleration command accelerates in the positive direction. This does not take advantage of the space the spring has to decompress but also uses less power.

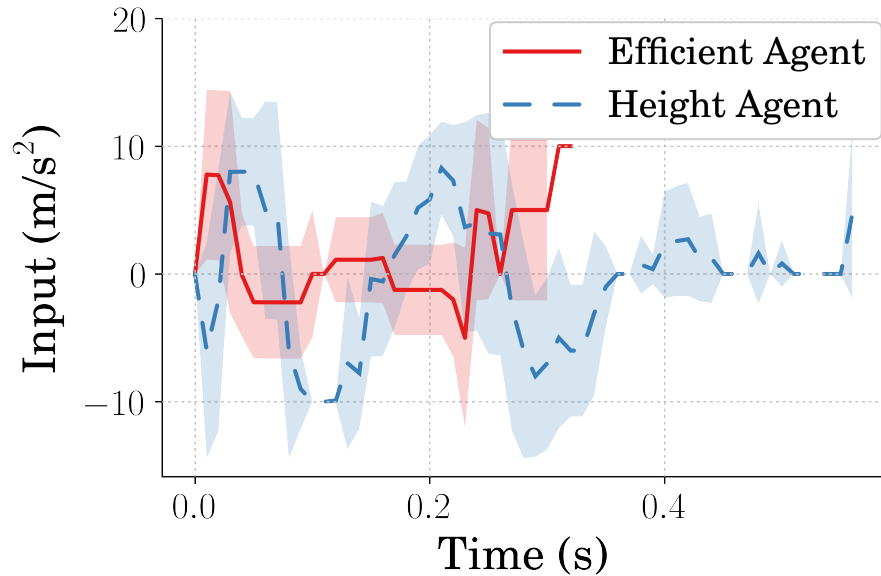


**Figure 28.** Average Input Performance

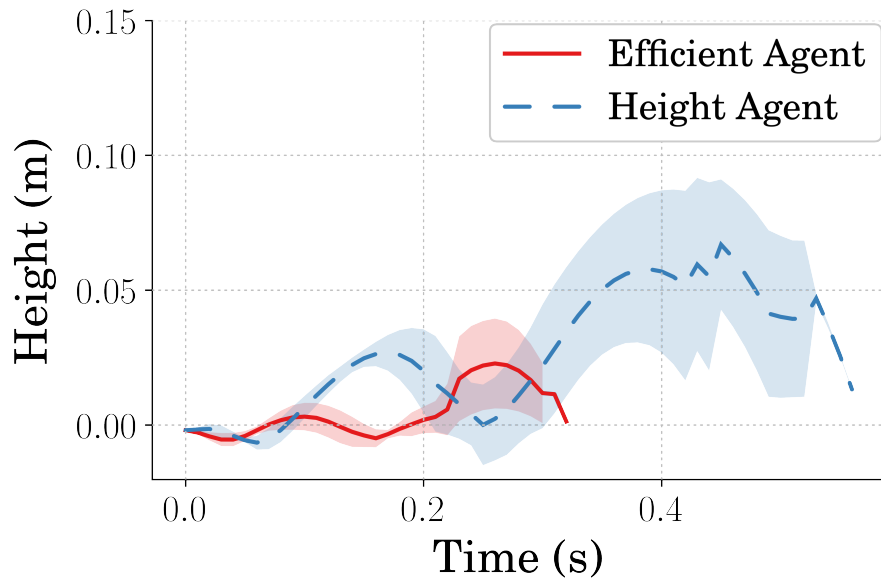


**Figure 29.** Average Jumping Performance

Average jumping performance for the efficient and high command types are shown in Figure 29. It is firstly obvious that the high jumping controllers learned a command that jumped the monopode significantly higher. It can be seen as well, as the input suggested, the efficient controllers learned a policy that did not utilize the spring decompression available.

## 5.7 Conclusion

The conclusion.

## VI Appendix: Concurrent Design Algorithm

The algorithm presented, is in simple terms, an instantiation of the TD3 algorithm within an instantiation of the TD3 algorithm. Line 18, highlighted with green text, denotes the start of the inner loop and is responsible for learning a mechanical design similar to what is shown in Chapter 4. This inner loop runs before the control policy is updated depending on a hyperparameter that is related to how often the mechanical design should be updated. What wraps the green text, is considered the outer loop, and is responsible for learning a control policy.

The inner and outer loop are concurrent in that the inner loop takes the policy being trained in the outer loop and uses it to simulate the environment to learn an optimal mechanical design. Once the design has been learned, the inner loop passes the design back to the outer loop so that it can modify the environment which it is using to train a control policy.

**6.0.1 Additional Hyperparameters.** This algorithm presents an additional hyperparameter on top of the ones already present, being the rate at which the design is updated within the outer loop (see blue text). Testing this hyperparameter has shown . . .

What happens when we change this hyperparameter?

Additionally, there are  $n$ , number of design updating policies instantiated within the inner loop. This is to better replicate the results found in Chapter 4 and to avoid issues where a single policy might find a local optimal design. In this work,  $n$  was set to 10 as it provided enough variation to keep a single bad policy from effecting the average design learned.

**6.0.2 Discrete vs. Continuous.** Additionally, there are two methods for implementing the inner loop. The first being at every instantiation, the policy

parameters learning a design (line 20) are initialized from nothing having no built intuition for good designs. To accomplish this, load would be removed from the description on line 20 of the algorithm. As for the second method, rather than starting with an untrained policy every design update, the policy is saved and then reloaded the next time the design is updated. During the first design update,  $n$  policies are created and learn a design. They are then saved along with their replay buffers so they can be reloaded to continue updating the mechanical design. . . .

Test this and get some results.

- 1: Input: initialize policy parameters  $\theta_{ctr}$ , Q-function parameters  $\phi_{1,ctr}$  and  $\phi_{2,ctr}$  and empty replay buffer,  $\mathcal{D}_{ctr}$
- 2: Set target parameters equal to main parameters:  $\theta_{ctr,targ} \leftarrow \theta$ ,  $\phi_{1,ctr,targ} \leftarrow \phi_{1,ctr}$ ,  $\phi_{2,ctr,targ} \leftarrow \phi_{2,ctr}$
- 3: **while** Not Converged **do**
- 4:     Observe system state  $s_{ctr}$  and select action  
 $a_{ctr} = \text{clip}(\mu_{\theta_{ctr}}(s_{ctr}) + \epsilon, a_{ctr,low}, a_{ctr,high}), \quad \epsilon \sim \mathcal{N}$
- 5:     Execute the action  $a$  in the environment
- 6:     Observe the next state  $s'_{ctr}$  and the reward  $r_{ctr}$  (verify if the state  $s'_{ctr}$  is a terminal state  $d_{ctr}$ )
- 7:     Store  $(s_{ctr}, a_{ctr}, r_{ctr}, s'_{ctr}, d_{ctr})$  in the replay buffer  $\mathcal{D}_{ctr}$
- 8:     **if**  $s'_{ctr}$  is terminal **then**
- 9:         Reset environment
- 10:      **end if**
- 11:     **if** Update Parameter % Update Frequency **then**
- 12:         **for**  $j$  in range number of updates **do**
- 13:             Sample random batch of transitions from buffer  $\mathcal{R}_{ctr}$
- 14:             Compute target actions:  
 $a_{ctr} = \text{clip}(\mu_{\theta_{ctr,targ}}(s'_{ctr}) + \text{clip}(\epsilon, -c, c), a_{ctr,low}, a_{ctr,high}), \quad \epsilon \sim \mathcal{N}(0, \sigma)$

15: Compute targets:  

$$y(r_{ctr}, s'_{ctr}, d_{ctr}) = r_{ctr} + \gamma (1 - d_{ctr}) \min_{i=1,2} Q_{\phi_{ctr,targ,i}}(s'_{ctr}, a_{ctr}(s'_{ctr}))$$
 16: Update the Q-function by way of gradient decent:  

$$\nabla_{\theta_{ctr}} \frac{1}{|B|} \sum_{(s_{ctr}, a_{ctr}, r_{ctr}, s'_{ctr}, d_{ctr}) \in B} (Q_{\phi_{ctr,i}}(s_{ctr}, a_{ctr}) - y(r_{ctr}, s'_{ctr}, d_{ctr}))^2 \quad \text{for } i = 1, 2$$
 17: **if**  $j$  % Policy Delay is 0 **then**  
 18:     **if** Update Design % Update Frequency **then**  
 19:         **for**  $i$  in range  $n$  instantiations of a mechanal design policy **do**  
 20:             Input: initialize/load policy parameters  $\theta_{des}$ , Q-function  
 parameters  $\phi_{1,des}$  and  $\phi_{2,des}$  and empty replay buffer,  $\mathcal{D}_{des}$   
 21:             Set target parameters equal to main parameters:  $\theta_{des,targ} \leftarrow \theta$ ,  
 $\phi_{1,des,targ} \leftarrow \phi_{1,des}$ ,  $\phi_{2,des,targ} \leftarrow \phi_{2,des}$   
 22:         **while** Not Converged **do**  
 23:             Observe system state  $s_{des}$  and select a design  
 $a_{des} = \text{clip}(\mu_{\theta_{des}}(s_{des}) + \epsilon, a_{des,low}, a_{des,high}), \quad \epsilon \sim \mathcal{N}$   
 24:             Simulate the design  $a$  in the environment using  $\pi_{\theta_{ctr}}$   
 25:             Observe the simulation  $s'_{des}$  and the reward  $r_{des}$  (verify if  
 the state  $s'_{des}$  is a terminal state  $d_{des}$ )  
 26:             Store  $(s_{des}, a_{des}, r_{des}, s'_{des}, d_{des})$  in the replay buffer  $\mathcal{D}_{des}$   
 27:         **if**  $s'_{des}$  is terminal **then**  
 28:             Reset environment  
 29:         **end if**  
 30:         **if** Update Parameter % Update Frequency **then**  
 31:             **for**  $j$  in range number of updates **do**  
 32:             Sample random batch of transitions from buffer  $\mathcal{R}_{des}$   
 33:             Compute target actions:  

$$a_{des} = \text{clip}(\mu_{\theta_{des,targ}}(s'_{des}) + \text{clip}(\epsilon, -c, c), a_{des,low}, a_{des,high}), \quad \epsilon \sim \mathcal{N}(0, \sigma)$$

34: Compute targets:  

$$y(r_{des}, s'_{des}, d_{des}) = r_{des} + \gamma (1 - d_{des}) \min_{i=1,2} Q_{\phi_{des,targ,i}}(s'_{des}, a_{des}(s'_{des}))$$
 35: Update the Q-function by way of gradient decent:  

$$\nabla_{\theta_{des}} \frac{1}{|B|} \sum_{(s_{des}, a_{des}, r_{des}, s'_{des}, d_{des}) \in B} (Q_{\phi_{des,i}}(s_{des}, a_{des}) - y(r_{des}, s'_{des}, d_{des}))^2 \quad \text{for } i = 1, 2$$
 36: **if**  $j$  % Policy Delay is 0 **then**  
 37:     Update policy by one step of gradient decent:  

$$\nabla_{\theta_{des}} \frac{1}{|B|} \sum_{s_{des} \in B} Q_{\phi_{des,1}}(s_{des}, \mu_{\theta_{des}}(s_{des}))$$
 38:     Update target networks by:  

$$\phi_{des,targ,i} \leftarrow \rho \phi_{des,targ,i} + (1 - \rho) \phi_{des,i} \quad \text{for } i = 1, 2$$

$$\theta_{targ} \leftarrow \rho \theta_{targ} + (1 - \rho) \theta$$
 39:     **end if**  
 40:     **end for**  
 41:     **end if**  
 42:     **end while**  
 43: Capture the final design that was learned as  $d_i$   
 44: **end for**  
 45: Compute the average of the designs:  

$$\mathbb{D} = \frac{\sum_{i=1}^n d_i}{n}$$
 46: **end if**  
 47: **Update the environment with the learned design  $\mathbb{D}$**   
 48: Update policy by one step of gradient decent:  

$$\nabla_{\theta_{ctr}} \frac{1}{|B|} \sum_{s_{ctr} \in B} Q_{\phi_{ctr,1}}(s_{ctr}, \mu_{\theta_{ctr}}(s_{ctr}))$$
 49: Update target networks by:  

$$\phi_{ctr,targ,i} \leftarrow \rho \phi_{ctr,targ,i} + (1 - \rho) \phi_{ctr,i} \quad \text{for } i = 1, 2$$

$$\theta_{ctr,targ} \leftarrow \rho \theta_{ctr,targ} + (1 - \rho) \theta_{ctr}$$
 50: **end if**

51:       **end for**

52:       **end if**

53: **end while**

## Bibliography

- [1] FOLKERTSMA, G. A., KIM, S., and STRAMIGIOLI, S., “Parallel stiffness in a bounding quadruped with flexible spine,” *IEEE International Conference on Intelligent Robots and Systems*, pp. 2210–2215, 2012.
- [2] PARK, H. W., WENSING, P. M., and KIM, S., “High-speed bounding with the MIT Cheetah 2: Control design and experiments,” *International Journal of Robotics Research*, vol. 36, no. 2, pp. 167–192, 2017.
- [3] SEOK, S., WANG, A., CHUAH, M. Y., HYUN, D. J., LEE, J., OTTEN, D. M., LANG, J. H., and KIM, S., “Design principles for energy-efficient legged locomotion and implementation on the MIT Cheetah robot,” *IEEE/ASME Transactions on Mechatronics*, vol. 20, no. 3, pp. 1117–1129, 2015.
- [4] BLACKMAN, D. J., NICHOLSON, J. V., PUSEY, J. L., AUSTIN, M. P., YOUNG, C., BROWN, J. M., and CLARK, J. E., “Leg design for running and jumping dynamics,” *2017 IEEE International Conference on Robotics and Biomimetics, ROBIO 2017*, vol. 2018-Janua, pp. 2617–2623, 2018.
- [5] SUGIYAMA, Y. and HIRAI, S., “Crawling and jumping of deformable soft robot,” *2004 IEEE/RSJ International Conference on Intelligent Robots and Systems (IROS)*, vol. 4, no. c, pp. 3276–3281, 2004.
- [6] GALLOWAY, K. C., CLARK, J. E., YIM, M., and KODITSCHEK, D. E., “Experimental investigations into the role of passive variable compliant legs for dynamic robotic locomotion,” *Proceedings - IEEE International Conference on Robotics and Automation*, pp. 1243–1249, 2011.
- [7] HURST, J., “The Role and Implementation of Compliance in Legged Locomotion,” *The International Journal of Robotics Research*, vol. 25, no. 4, p. 110, 2008.
- [8] PRATT, G. A. and WILLIAMSON, M. M., “Series elastic actuators,” *IEEE International Conference on Intelligent Robots and Systems*, vol. 1, pp. 399–406, 1995.
- [9] AHMADI, M. and BUEHLER, M., “Stable control of a simulated one-legged running robot with hip and leg compliance,” *IEEE Transactions on Robotics and Automation*, vol. 13, no. 1, pp. 96–104, 1997.
- [10] KANI, M. H. H. and AHMADABADI, M. N., “Comparing effects of rigid, flexible, and actuated series-elastic spines on bounding gait of quadruped robots,” pp. 282–287, 2013.
- [11] HORIGOME, A., QUDSI, Y., FISHER, E., and VAUGHAN, J., “Robot Jumping with Curved-Beam Flexible Legs Orange marker Blue marker Tether,”
- [12] LUO, Z.-H., “Direct Strain Feedback Control of Flexible Robot Arms: New Theoretical and Experimental Results,” vol. 38, no. 11, 1993.

- [13] HE, W., GAO, H., ZHOU, C., YANG, C., and LI, Z., “Reinforcement Learning Control of a Flexible Two-Link Manipulator: An Experimental Investigation,” *IEEE Transactions on Systems, Man, and Cybernetics: Systems*, pp. 1–11, 2020.
- [14] LILICRAP, T. P., HUNT, J. J., PRITZEL, A., HEESS, N., EREZ, T., TASSA, Y., SILVER, D., and WIERSTRA, D., “Continuous control with deep reinforcement learning,” *4th International Conference on Learning Representations, ICLR 2016 - Conference Track Proceedings*, 2016.
- [15] DWIEL, Z., CANDADAI, M., and PHIELIPP, M., “On Training Flexible Robots using Deep Reinforcement Learning,” *IEEE International Conference on Intelligent Robots and Systems*, pp. 4666–4671, 2019.
- [16] LI, Q., ZHANG, W. J., and CHEN, L., “Design for control - A concurrent engineering approach for mechatronic systems design,” *IEEE/ASME Transactions on Mechatronics*, vol. 6, no. 2, pp. 161–169, 2001.
- [17] CHEN, T., HE, Z., and CIOCARLIE, M., “Hardware as Policy: Mechanical and computational co-optimization using deep reinforcement learning,” *arXiv*, no. CoRL, 2020.
- [18] SCHAFF, C., YUNIS, D., CHAKRABARTI, A., and WALTER, M. R., “Jointly learning to construct and control agents using deep reinforcement learning,” *Proceedings - IEEE International Conference on Robotics and Automation*, vol. 2019-May, pp. 9798–9805, 2019.
- [19] WHITMAN, J., BHIRANGI, R., TRAVERS, M., and CHOSET, H., “Modular Robot Design Synthesis with Deep Reinforcement Learning,” *Proceedings of the AAAI Conference on Artificial Intelligence*, vol. 34, no. 06, pp. 10418–10425, 2020.
- [20] ZHAO, W., QUERALTA, J. P., and WESTERLUND, T., “Sim-to-Real Transfer in Deep Reinforcement Learning for Robotics: A Survey,” *2020 IEEE Symposium Series on Computational Intelligence, SSCI 2020*, pp. 737–744, 2020.
- [21] VECERIK, M., HESTER, T., SCHOLZ, J., WANG, F., PIETQUIN, O., PIOT, B., HEESS, N., ROTHÖRL, T., LAMPE, T., and RIEDMILLER, M., “Leveraging Demonstrations for Deep Reinforcement Learning on Robotics Problems with Sparse Rewards,” pp. 1–10, 2017.
- [22] PLAPPERT, M., ANDRYCHOWICZ, M., RAY, A., MCGREW, B., BAKER, B., POWELL, G., SCHNEIDER, J., TOBIN, J., CHOCIEJ, M., WELINDER, P., KUMAR, V., and ZAREMBA, W., “Multi-Goal Reinforcement Learning: Challenging Robotics Environments and Request for Research,” pp. 1–16, 2018.
- [23] FUJIMOTO, S., VAN HOOF, H., and MEGER, D., “Addressing Function Approximation Error in Actor-Critic Methods,” *35th International Conference on Machine Learning, ICML 2018*, vol. 4, pp. 2587–2601, 2018.

- [24] SUTTON, R. S. and MATHEUS, C. J., “Learning Polynomial Functions by Feature Construction,” *Machine Learning Proceedings 1991*, pp. 208–212, 1991.
- [25] WATKINS, C., “Learning From Delayed Rewards,” 1989.
- [26] MNIH, V. and SILVER, D., “Playing Atari with Deep Reinforcement Learning,” pp. 1–9.
- [27] DORMANN, A. R., HILL, A., GLEAVE, A., KANERVISTO, A., ERNESTUS, M., and NOAH, “Stable-Baselines3: Reliable Reinforcement Learning Implementations,” *Journal of Machine Learning Research*, vol. 22, no. 22, pp. 1–8, 2021.
- [28] PASZKE, ADAM AND GROSS, SAM AND MASSA, FRANCISCO AND LERER, ADAM AND BRADBURY, JAMES AND CHANAN, GREGORY AND KILLEEN, TREVOR AND LIN, ZEMING AND GIMELSHEIN, NATALIA AND ANTIGA, LUCA AND DESMAISON, ALBAN AND KOPF, ANDREAS AND YANG, EDWARD AND DEVITO, ZACHA, S., *PyTorch: An Imperative Style, High-Performance Deep Learning Library*. Curran Associates, Inc., 2019.
- [29] HA, S., XU, P., TAN, Z., LEVINE, S., and TAN, J., “Learning to walk in the real world with minimal human effort,” *arXiv*, no. CoRL, pp. 1–11, 2020.
- [30] FANKHAUSER, P., HUTTER, M., GEHRING, C., BLOESCH, M., HOEPFLINGER, M. A., and SIEGWART, R., “Reinforcement learning of single legged locomotion,” *IEEE International Conference on Intelligent Robots and Systems*, pp. 188–193, 2013.
- [31] XIAO, Q., CAO, Z., and ZHOU, M., “Learning locomotion skills via model-based proximal meta-reinforcement learning,” *Conference Proceedings - IEEE International Conference on Systems, Man and Cybernetics*, vol. 2019-Octob, pp. 1545–1550, 2019.
- [32] HAARNOJA, T., HA, S., ZHOU, A., TAN, J., TUCKER, G., and LEVINE, S., “Learning to Walk Via Deep Reinforcement Learning,” 2019.
- [33] TSOUNIS, V., ALGE, M., LEE, J., FARSHIDIAN, F., and HUTTER, M., “DeepGait: Planning and control of quadrupedal gaits using deep reinforcement learning,” *arXiv*, no. 1, pp. 1–8, 2019.
- [34] DA, X., XIE, Z., HOELLER, D., BOOTS, B., ANANDKUMAR, A., ZHU, Y., BABICH, B., and GARG, A., “Learning a Contact-Adaptive Controller for Robust, Efficient Legged Locomotion,” vol. 1, no. c, 2020.
- [35] BLICKHAN, R. and FULL, R. J., “Similarity in multilegged locomotion: Bouncing like a monopode,” *Journal of Comparative Physiology A*, vol. 173, no. 5, pp. 509–517, 1993.
- [36] BROCKMAN, G., CHEUNG, V., PETTERSSON, L., SCHNEIDER, J., SCHULMAN, J., TANG, J., and ZAREMBA, W., “OpenAI Gym,” pp. 1–4, 2016.

- [37] HARPER, M. Y., NICHOLSON, J. V., COLLINS, E. G., PUSEY, J., and CLARK, J. E., “Energy efficient navigation for running legged robots,” *Proceedings - IEEE International Conference on Robotics and Automation*, vol. 2019-May, pp. 6770–6776, 2019.
- [38] PACE, J., HARPER, M., ORDONEZ, C., GUPTA, N., SHARMA, A., and COLLINS, E. G., “Experimental verification of distance and energy optimal motion planning on a skid-steered platform,” *Unmanned Systems Technology XIX*, vol. 10195, p. 1019506, 2017.
- [39] VAUGHAN, J., “Jumping Commands For Flexible-Legged Robots,” 2013.
- [40] SORENSEN, K. L. and SINGHOSE, W. E., “Command-induced vibration analysis using input shaping principles,” *Autom.*, vol. 44, pp. 2392–2397, 2008.
- [41] SINGER, N. C. and SEERING, W. P., “Preshaping Command Inputs to Reduce System Vibration,” *Journal of Dynamic Systems, Measurement, and Control*, vol. 112, no. 1, pp. 76–82, 1990.
- [42] SINGHOSE, W., SEERING, W., and SINGER, N., “Residual Vibration Reduction Using Vector Diagrams to Generate Shaped Inputs,” *Journal of Mechanical Design*, vol. 116, no. 2, pp. 654–659, 1994.
- [43] LUCK, K. S., AMOR, H. B., and CALANDRA, R., “Data-efficient co-adaptation of morphology and behaviour with deep reinforcement learning,” *arXiv*, no. CoRL, 2019.
- [44] HA, D., “Reinforcement learning for improving agent design,” *Artificial Life*, vol. 25, no. 4, pp. 352–365, 2019.
- [45] WANG, T., ZHOU, Y., FIDLER, S., and BA, J., “Neural graph evolution: Towards efficient automatic robot design,” *arXiv*, pp. 1–17, 2019.
- [46] HU, S., YANG, Z., and MORI, G., “Neural fidelity warping for efficient robot morphology design,” *arXiv*, 2020.

Albright, Andrew. Bachelor of Science, North Carolina State University, Spring 2020;  
Masters of Science, University of Louisiana at Lafayette, Spring 2022

Major: Mechanical Engineering

Title of Thesis: Mechanical Design and Control of Flexible-Legged Jumping Robots

Thesis Director: Dr. Joshua E. Vaughan

Pages in Thesis: 125; Words in Abstract: 185

## **Abstract**

Loreum ipsum dolor sit amet, consectetur adipiscing elit. Vivamus nec tellus eget  
elit aliquet accumsan sit amet in lacus. In hac habitasse platea dictumst. Ut sit amet  
elit odio. Aenean lobortis mollis metus, sed consequat neque tristique in. Curabitur nec  
hendrerit metus. Praesent non scelerisque urna, vitae iaculis diam. Aliquam nisl est,  
imperdiet eu nulla sed, bibendum pulvinar arcu. In ultricies purus purus, vulputate  
congue justo volutpat ut. Donec nunc magna, rutrum nec turpis et, viverra efficitur  
lorem. In hac habitasse platea dictumst. Vestibulum maximus lobortis nisl, eget  
molestie sem sollicitudin nec. Mauris ut enim eu ipsum auctor rhoncus ac vel eros.

Vivamus tincidunt, tortor eu rutrum dapibus, orci turpis porta metus, ac iaculis  
quam eros sollicitudin nisl. Nam id massa elementum, commodo mi at, lobortis nisl.  
Fusce vestibulum eu lorem non aliquam. Morbi eleifend tortor id metus elementum, ac  
tincidunt lorem commodo. Pellentesque vestibulum, erat in tempus vehicula, ex urna  
auctor leo, ut lobortis eros mauris nec erat. Aliquam erat volutpat. Sed sed pretium  
risus.

## **Biographical Sketch**

Forrest Montgomery was born in Lafayette, Louisiana for all intents and purposes. He began his academic career at the University of Louisiana with an internal struggle between majoring in Mechanical Engineering or Industrial Design. This thesis is evident of the choice he made. After earning his Bachelor's degree at the University of Louisiana at Lafayette in the Spring of 2015, he joined the CRAWLAB and conducted research in dynamics, controls, and robotics under the tutelage of Dr. Joshua Vaughan. This research culminated with earning a Master's degree in Mechanical Engineering again at the University of Louisiana at Lafayette in the Summer of 2017.